A 4-year zonal climatology of lower tropospheric CO_2 derived from ocean-only Atmospheric Infrared Sounder observations

L. Larrabee Strow[1] and Scott E. Hannon[1]

Received 14 December 2007; revised 18 March 2008; accepted 29 May 2008; published 20 September 2008.

[1] A 4-year zonally averaged climatology of atmospheric CO_2, ocean only, between ±60° latitude has been derived from the Atmospheric Infrared Sounder (AIRS) radiances. Using only very clear fields of view, the CO_2 profile in the computed radiances is scaled until agreement is found with observations. ECMWF forecast and analysis fields are used for the temperature profile in the computed radiances. The AIRS channels used to derive CO_2 amounts are nominally sensitive to CO_2 variability in the ~300–800 mbar region (2–9 km), significantly lower in the atmosphere than that in previous studies using AIRS. Validation using aircraft measurements of CO_2 at 650 mbar indicates that the AIRS CO_2 results presented here are accurate to the 0.5–1.0 ppm level. The AIRS-derived climatology clearly exhibits the CO_2 rectifier effect, with mean CO_2 values several parts per million lower than in those in the boundary layer. The AIRS CO_2 seasonal cycle has a relatively constant amplitude of ~3 ppm from +10° to +60° latitude, which matches the boundary layer seasonal cycle amplitude near +10° latitude but is about three times smaller than that in the boundary layer amplitude at +60° latitude. Phase comparisons between the AIRS and boundary layer CO_2 seasonal cycles show the boundary layer phase leading AIRS in the Northern Hemisphere until ~+10° latitude, where the phases cross and the AIRS higher-altitude CO_2 begins to lead the boundary layer phase down to ~−10° latitude. These results may offer new insight into CO_2 interhemispherical transport. Growth rates derived from the AIRS CO_2 climatology are 2.21 ± 0.24 ppm/year, in good agreement with in situ measurements.

Citation: Strow, L. L., and S. E. Hannon (2008), A 4-year zonal climatology of lower tropospheric CO_2 derived from ocean-only Atmospheric Infrared Sounder observations, *J. Geophys. Res.*, *113*, D18302, doi:10.1029/2007JD009713.

1. Introduction

[2] Atmospheric CO_2 is the primary radiative forcing greenhouse gas, and its atmospheric growth rate has been rising steadily in the past few decades because of increasing global emissions [*Raupach et al.*, 2007]. Reliable estimates of climate change depend upon our ability to forecast atmospheric CO_2 concentrations, which requires knowledge of the CO_2 sources, sinks, and atmospheric transport. Inversion studies, [see, for example *Denning et al.*, 1995; *Gurney et al.*, 2003] generally use relatively sparse in situ boundary-layer CO_2 measurements, coupled with an atmospheric transport model to estimate source and sink regions and fluxes. Input data for these studies are relatively sparse, and heavily weighted to the Northern Hemisphere land sites. Constraining CO_2 sinks with existing data has been especially difficult since sinks involve large geographic areas, including the oceans. Moreover, transport of CO_2 from the boundary layer to the free troposphere is not well understood, but may be key for identification of sink regions.

[3] Two very recent studies [*Stephens et al.*, 2007; *Yang et al.*, 2007] emphasized the importance of using information on the vertical extent of CO_2 to further constrain transport and flux models. *Stephens et al.* [2007] found that only three (out of twelve) TransCom 3 transport models [*Gurney et al.*, 2003] could closely reproduce the CO_2 vertical distribution derived from a rather limited number of aircraft flights. These three particular models predicted very different flux estimates than the other nine models, strongly suggesting a weaker northern uptake of CO_2 and weaker tropical emission than previous "consensus estimates".

[4] *Yang et al.* [2007] also found that the growing season net flux in the Northern Hemisphere is ~28% larger than predicted by models using column-averaged mixing ratios of CO_2 and partial columns derived from aircraft profiles, rather than boundary layer values. They attributed this new result to their use of the column CO_2 as the primary measurement, since it is less sensitive to vertical mixing errors in the transport models.

[5] Sufficiently accurate satellite measurements of CO_2 would greatly enhance our understanding of the global carbon cycle, by providing a much higher spatial and temporal data density. Profile information from satellite measurements may also be able to enhance the improvements discussed above by *Stephens et al.* [2007] and *Yang et al.* [2007]. Near infrared remote sensing of CO_2 can provide the

[1]Physics Department and Joint Center for Earth Systems Technology, University of Maryland Baltimore County, Baltimore, Maryland, USA.

0148-0227/08/2007JD009713

atmospheric CO_2 column [*Barkley et al.*, 2007; *Buchwitz et al.*, 2007a, 2007b; *Houweling et al.*, 2005], while infrared sounders can potentially measure CO_2 in the free troposphere [*Chédin et al.*, 2003a, 2003b; *Engelen et al.*, 2004; *Engelen and McNally*, 2005; *Crevoisier et al.*, 2004; *Chahine et al.*, 2005]. Both of these measurements, separately, or in combination [*Barkley et al.*, 2006b], could potentially contribute to our understanding of the global climate budget if they had sufficient accuracy and well understood error characteristics.

1.1. This Work

[6] We present here a new 4-year zonally-averaged climatology of lower-tropospheric CO_2 derived from the Atmospheric Infrared Sounder (AIRS) flying on NASA's Aqua satellite. This climatology is restricted to clear, ocean-only observations in the $\pm 60^\circ$ latitude range. What distinguishes this work from previous AIRS retrievals of CO_2 is our use of channels that peak at $\sim$550 mbar, rather than near $\sim$200 mbar, with a continuous 4-year climatology that allows accurate measurements of growth rates and seasonal variability as a function of latitude.

[7] Our primary measurement uses only a single AIRS channel sensitive to CO_2, centered at 791.7 cm^{-1}, because of its combined low sensitivity to temperature and high sensitivity to CO_2. We distinguish between temperature and CO_2 variations by using European Center for Medium-range Weather Forecasts (ECMWF) analysis/forecast model data for the atmospheric temperature profile. This overcomes one of the major difficulties in AIRS-only retrievals of CO_2, but, of course, makes our results dependent on the accuracy of the ECMWF fields. We perform similar retrievals of CO_2 with AIRS using channels in the 2400 cm^{-1} region that are more sensitive to temperature than the 791.7 cm^{-1} channel, and use the difference in the CO_2 product from these two spectral regions as a diagnostic on the accuracy of the ECMWF temperature fields. In this paper we will often refer to the 791 cm^{-1} region as long-wave, LW, and the 2400 cm^{-1} region as short-wave, SW.

[8] The CO_2 variability reported here represents very small signatures in the AIRS radiances. The brightness temperature of the more sensitive 791.7 cm^{-1} channel only decreases by approximately -0.03 K for a 1 ppm positive offset of the CO_2 profile. The 2400 cm^{-1} channels are even less sensitive to CO_2. The full range of CO_2 values derived from the AIRS spectra for the four years examined here is 18 ppm, which only represents a brightness temperature range of 0.54 K. The results presented here therefore highlight the extreme stability of both the AIRS instrument and the ECMWF model fields.

[9] A major advantage of our simple approach using clear-only fields of view is the ability to easily process, and re-process, this 4-year data set. Partial validation of our climatology is made by comparison to the NOAA GLOBALVIEW [*GLOBALVIEW-CO2*, 2006] aircraft flights over ocean, and the GLOBALVIEW Marine Boundary Layer (MBL) CO_2 product, which is a smoothed zonal representation of a large number of globally distributed in situ measurements and has an estimated accuracy of $\sim$0.3 ppm. The comparisons to MBL help establish the plausibility of our results and stimulate further investigations. In this work we introduce our retrieval methods and validation, comparisons to global CO_2 models will be presented in a forthcoming paper.

1.2. Previous Work

[10] Infrared sensing of CO_2 began with the pioneering work of *Chédin et al.* [2002, 2003b] using the NOAA/TOVS infrared sounder. The more recent work of *Chédin et al.* [2003b] used a neural network retrieval approach that could differentiate between temperature and CO_2 by including Microwave Sounding Unit (MSU) radiances in the process, since MSU radiance are independent of CO_2 but not temperature. Their infrared CO_2 Jacobians peaked at $\sim$300 mbar, and they analyzed 4 years covering the 1987–1991 time frame between $\pm 20^\circ$ latitude. Their measurement standard deviations were about 3 ppm. They also successfully retrieved mean CO_2 growth rates over the $\pm 20^\circ$ latitude range of $\sim$1.75 ppm/year that agreed quite well with in situ measurements.

[11] The SCIAMACHY instrument on ENVISAT allows the measurement of the CO_2 column, mostly over land, with a precision that gives agreement with models to within $\sim$2 ppm for the amplitude of Northern Hemisphere seasonal cycles. The SCIAMACHY measurements may have biases of 4% or less [*Barkley et al.*, 2007], which are difficult to assess because of the relatively high variability of CO_2 over land sites and the lack of in situ data. Recently *Buchwitz et al.* [2007a, 2007b] measured the CO_2 rate of growth for the 2003–2006 time period with SCIAMACHY, and found agreement with the NOAA CarbonTracker [*Peters et al.*, 2007] in the 1 ppm/year range. At present, it is not clear if the SCIAMACHY data is sufficiently unbiased, or has well enough characterized errors, to be used for inverse modeling of CO_2 [*Barkley et al.*, 2006a; *Tiwari et al.*, 2006].

[12] AIRS (Atmospheric Infrared Sounder) [*Aumann et al.*, 2003] on NASA's Aqua satellite platform provides a wealth of high-spectral resolution channels with sensitivity to CO_2, but with limited boundary-layer information, unlike SCIAMACHY. However, AIRS does have the ability to potentially provide several independent pieces of information on the CO_2 profile above the boundary layer.

[13] A number of previous studies have used AIRS channels peaking in the upper troposphere (200 mbar range) to retrieve CO_2 [*Engelen et al.*, 2004; *Engelen and McNally*, 2005; *Crevoisier et al.*, 2004; *Chahine et al.*, 2005]. These nominal 200 mbar measurements make them significantly less sensitive to the immediate effects of CO_2 sources and sinks. They are more dependent on transport, and could possibly be used to constrain transport model biases, although *Chevallier et al.* [2005] suggest that the AIRS CO_2 biases must be kept to a few tenths of a ppm for assimilation into a transport model.

[14] The most comprehensive AIRS CO_2 product by *Engelen and McNally* [2005] covers a period of 15 months. They quote monthly *random* mean errors of 1–6 ppm (1–3 ppm for the latitudes reported in this paper). *Tiwari et al.* [2006] have made detailed comparisons between a model and their retrievals with qualitatively good agreement, especially for amplitude of the seasonal cycles. However, the transport model shows significant growth of CO_2 in the Northern Hemisphere winter that is absent in their AIRS CO_2 weighted column [see *Tiwari et al.*, 2006, Figure 8].

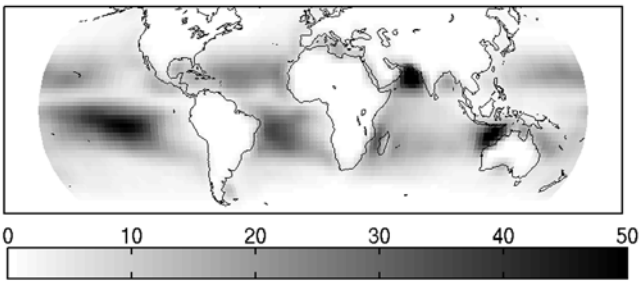

Figure 1. Density plot (in units of 1000) of clear AIRS FOVs used to derive the AIRS CO_2.

Our lower altitude CO_2 product reported here does indeed show this Northern Hemisphere winter growth of CO_2.

[15] *Chahine et al.* [2005] introduced an independent CO_2 retrieval using AIRS that also uses channels that peak in the ~300 mbar region. He reports results for two years of AIRS match ups with the JAL airline measurements [*Matsueda et al.*, 2002], with a monthly mean standard deviation of 1.2 ppm.

[16] The neural-network approach of *Chédin et al.* [2003a] has also been applied to AIRS by *Crevoisier et al.* [2004] using channels with the CO_2 Jacobian peaking at ~200 mbar. They analyzed seven months of data in the ±20° latitude range with an estimated precision of 2.1–2.5 ppm for monthly means with 15° × 15° spatial averaging. They indicate low biases, ~0.9 ppm, relative to the work of *Matsueda et al.* [2002] (JAL using GLOBALVIEW terminology).

[17] Finally, *Aumann et al.* [2005] tracked two AIRS channels over time between ±30° latitude. One channel is mainly sensitive to N_2O only, while the other channel is dominated by CO_2. He showed that if you assume an N_2O growth rate, that the relative change in radiance in these two channels lead to a CO_2 growth rate that agrees very well with in situ measurements.

[18] In summary, although there have been a number of satellite measurements of atmospheric CO_2, they have either probed the middle to upper troposphere (200–300 mbar peak sensitivities) or have measured the atmospheric CO_2 column (using near-infrared sensors which work primarily over land). The results presented here, although only over ocean, are the first to use thermal infrared satellite data to measure CO_2 in the lower-troposphere. In addition, our CO_2 retrievals cover a much longer time span, with higher accuracy, than previous infrared remote sensing studies. This comprehensive ocean climatology allows detailed analysis of the latitude dependence of the lower-tropospheric CO_2 seasonal cycle amplitude and phase, and of CO_2 growth rates.

2. AIRS Satellite Data

[19] AIRS measures 2378 high-spectral resolution infrared radiances between 650 and 2665 cm^{-1} with a nominal resolving power ($\lambda/\Delta\lambda$) of 1200 and nadir footprint of 13 km. Flying on board NASA's EOS Aqua spacecraft, AIRS has been operational since September 2002, supplying almost continuous global measurements twice each day in a sun-synchronous orbit with very stable equator crossing times of 1:30 am and 1:30 pm, and 705 km orbital altitude. AIRS primary purpose was to improve operational weather forecasting [*Chahine et al.*, 2006], but the excellent stability of AIRS is now allowing studies related to climate and monitoring of atmospheric composition.

[20] The CO_2 climatology reported here is derived from AIRS night-only, clear fields of view (FOVs), over ocean. The algorithm for selecting clear FOVs has been previously described by *Strow et al.* [2006], and is primarily based on a uniformity filter and several spectral tests. This filter is very similar to one described by *Aumann et al.* [2006], and returns only about 1% of all ocean observations. Following *Aumann et al.* [2006], we estimate that our clear FOVs have a residual amount of cloud contamination that produces a nominal 0.2 K cold bias in the spectra.

[21] A density map of the FOVs returned by the clear detection algorithm shown in Figure 1 indicates that our individual samples are widely dispersed, although some locations are more intensively sampled because of prevailing clear conditions. Obviously, the reduction of statistical errors by zonal averaging may introduce sampling errors that can complicate the interpretation of the CO_2 climatology. This may be especially true for the Indian/Arabian Ocean where the Asian continent occupies the northern latitudes, giving more of a continental rather than ocean flavor to the CO_2 climatology.

[22] A main goal of this work is to derive CO_2 concentrations at lower altitudes than previous studies. The existing retrievals of CO_2 with AIRS used channels peaking in the 200–300 mbar region because the authors wished to avoid channels contaminated by either other trace gases or by surface emission. A comprehensive examination of contamination of AIRS channels has been performed in the work of *Crevoisier et al.* [2003] and *Chédin et al.* [2003a]. For example, Figure 6 of this last reference shows that many of the mid-tropospheric AIRS channels in the 700–780 cm^{-1} region have significant O_3 contamination. Many CO_2 channels have significant surface contamination that other investigators wished to avoid. *Crevoisier et al.* [2003] suggest a list of candidate channels for CO_2 retrievals in the wave number ranges from 664–741 cm^{-1} and 2249–2391 cm^{-1}, most of which have CO_2 Jacobians that peak far higher than the 791.7 cm^{-1} channel we use. The only low-peaking channels they selected are the 2388–2391 cm^{-1} SW channels. However, note that at present, actual CO_2 retrieval results have only been reported for channels peaking in the 200–300 mbar range.

[23] Since we use ECMWF for the temperature profile, we wish to minimize the effect of errors in the temperature profile. A useful metric for channel selections is the ratio

$$\frac{dBT/dCO_2}{dBT/dT} \tag{1}$$

where dT represents a uniform (1 K) offset to the air temperature profile and dCO_2 is a uniform (−10%) offset to the CO_2 profile. Here we wish to maximize sensitive to CO_2 while minimizing sensitivity to temperature profiles errors. Figure 2 plots this ratio for the 4 and 15 μm regions sensitive to CO_2. The AIRS channel centered at 791.7 cm^{-1} easily has the largest sensitivity ratio. Furthermore, Figure 3 shows that the CO_2 Jacobian for this channel peaks at ~500–550 mbar or ~5 km, rather than at 200–300 mbar,

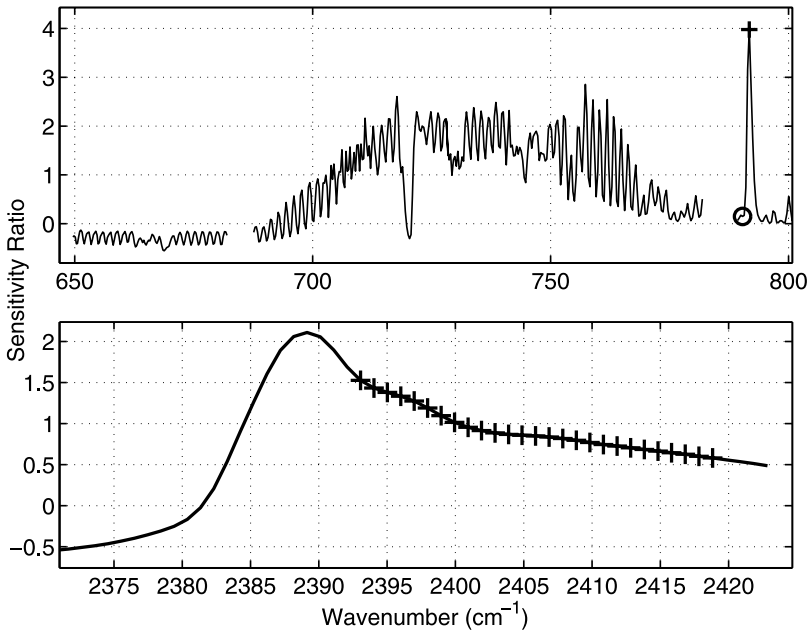

Figure 2. Ratios of CO_2 to profile temperature sensitivity in observed $B(T)$s or $(dBT/dCO_2)/(dBT/dT)$. T is the atmospheric temperature profile, which was shifted by a uniform 1 K offset. The CO_2 profile was decreased with a uniform −10% offset. In the top, the 791.7 cm^{-1} CO_2 channel is denoted with a plus, and the 790.3 cm^{-1} channel is denoted with a circle. The SW channels used to derive CO_2 are denoted with plus symbols in the bottom.

or 9–12 km, used in previous studies of CO_2 with AIRS [*Engelen et al.*, 2004; *Engelen and McNally*, 2005; *Crevoisier et al.*, 2004; *Chahine et al.*, 2005]. The 4 μm channels have a lower sensitivity ratio, around unity, partly because they are more temperature sensitive and partly because they are weaker transitions. However, as seen in Figure 3 the CO_2 Jacobians for these channels are quite similar to the 791.7 cm^{-1} CO_2 Jacobian, and probe the mid- to lower-troposphere. The channels used for our SW CO_2 retrieval stop at 2393 cm^{-1} because stratospheric sensitivity grows quickly as you move to lower wave numbers.

[24] Both the 791.7 cm^{-1} and 2400 cm^{-1} CO_2 channels will have significant surface contamination that must be properly modeled so it is not confused with CO_2. For the 791.7 cm^{-1} transition, a very close channel at 790.3 cm^{-1} has no CO_2 absorption and can be used to derive the

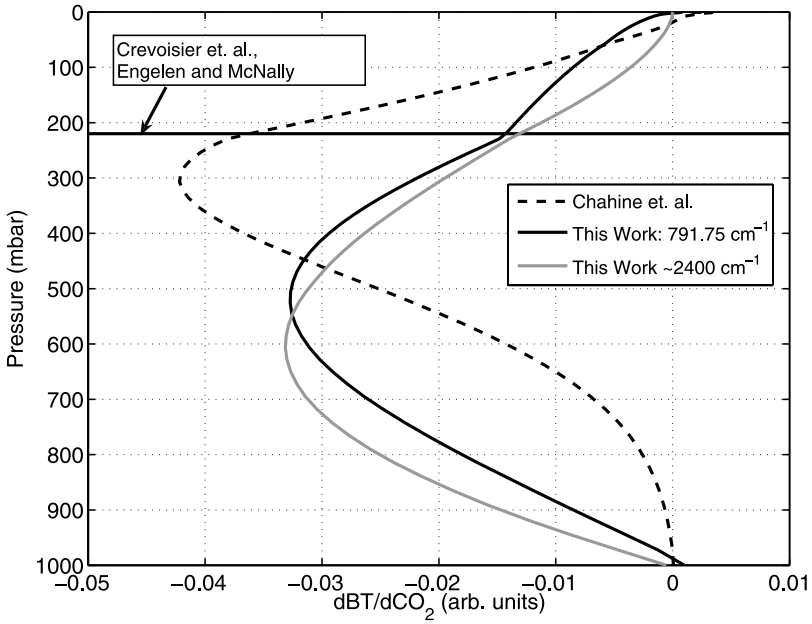

Figure 3. CO_2 Jacobians (dBT/dCO_2^1) for the channels used in this work and for the work of *Chahine et al.* [2005]. Also shown are the reported peak locations of the CO_2 Jacobians used by *Crevoisier et al.* [2004] and *Engelen and McNally* [2005].

effective surface emission for the 791.7 cm^{-1} channel. In the 2400 cm^{-1} region the CO_2 transmittance drops rapidly (but not to zero) past 2400 cm^{-1}, allowing a simultaneous retrieval of the effective surface emission and CO_2 column offset.

[25] Although the Masuda surface emissivity is quite accurate, the very stringent accuracy requirements for the CO_2 retrieval led us to re-estimate the effective surface temperature (which nominally includes the surface emissivity) close to the CO_2 channels. In addition, small residual effects of un-detected low clouds, and possibly improperly modeled water vapor continuum, may be present in our computed radiances. Since our 790.3 cm^{-1} surface channel is only 1.4 cm^{-1} away from the 791.7 cm^{-1} CO_2 channel, we assume these surface emissions are identical for these two channels. Similarly for the 2400 cm^{-1} region, we assume surface emissions are identical in the 2393–2418 cm^{-1} range used for the SW CO_2 retrieval.

[26] A major assumption of this work is that the ECMWF temperature fields are statistically accurate enough to allow meaningful CO_2 retrievals. We partially test this assumption by comparing the LW to SW CO_2 (see section 3.2). ECMWF uses radiosonde measurements as the "anchoring network" of observations for the ECMWF tropospheric temperatures [*Auligne et al.*, 2007], with no bias correction. This is in contrast to infrared satellite data assimilated by ECMWF (such as AIRS), which is bias-corrected to provide better agreement with the model and radiosondes. In large part the infrared satellite data is used to lower the standard deviation of the model rather than to provide model offsets.

[27] We also note that comparisons between ECMWF computed and observed AIRS radiances (for CO_2 dominant channels) generally have standard deviations that are almost equivalent to the AIRS instrument noise, indicating that ECMWF is tracking the true atmosphere temperatures very closely.

3. CO_2 Retrieval Method

[28] The starting point for our CO_2 retrieval are the nominally clear AIRS radiance observations, and the nearest matching ECMWF operational analysis or forecast model profiles. ECMWF provides an analysis at 00, 06, 12, and 18 UTC, 3-hour forecasts at 03, and 15 UTC, and 9 hour forecasts at 09 and 21 UTC. Prior to February 2006 these fields were on a T511L60 grid (0.5° lat/lon resolution, 60 vertical layers), which ECMWF subsequently upgraded to a T799L91 grid (0.25° lat/lon, 91 vertical layers).

[29] We first compute synthetic radiances using the ECMWF profile and sea-surface temperature, the Masuda sea surface emissivity model [*Masuda et al.*, 1988], and a default CO_2 amount of 370 ppm. The radiative transfer model used for these calculations is a stand-alone version of the AIRS operational radiative transfer algorithm, SARTA [*Strow et al.*, 2003, 2006]. In order to reduce bias errors due an inaccurate ECMWF SST or total column water (TCW), we first derive these quantities from the observed spectra. The fitted SST differs from the ECMWF SST because of the effects of evaporative cooling of the sea surface, and because of small amounts of residual cloud contamination.

[30] The SST and TCW fits use a combination of windows channels, and channels containing weak water vapor lines, all in the 2600 cm^{-1} region, as previously described [*Strow et al.*, 2006]. A number of window channels in this region contain only ~0.3 K of atmospheric absorption, and are therefore ideal for deriving an effective SST. We also simultaneously minimize the bias for several weak water line channels, giving us an improved TCW. The TCW is modified by scaling the ECMWF water vapor profile with a constant multiplier. A re-calculation of synthetic AIRS spectra using these two new parameters lowers the standard deviation of the biases in the LW (10–12 μm) by a factor of three. Our mean (±45° latitude) TCW agrees with the ECWMF model TCW to ~3%.

[31] The CO_2 amount is retrieved by a linear least-squares fit of the following set of equations that relate the bias to the derivatives of the brightness temperature for channel i, the CO_2 column scaling factor, δCO_2, and effective surface temperature offset δT_s,

$$BT_i^{obs} - BT_i^{cal}(\mathrm{ECMWF}) = \frac{dB_i}{dCO_2}\delta CO_2 + \frac{dB_i}{dT_s}\delta T_s. \quad (2)$$

For the LW CO_2 climatology we use only two channels, while for the SW climatology we use 26 channels. The LW and SW climatologies are completely separate products, each derived from simultaneous fits of the above equation to only LW channels, or, to only SW channels. Validation and detailed analysis presented here uses only the LW CO_2 climatology, which we consider more accurate.

[32] All computed brightness temperatures, and their surface and CO_2 derivatives were computed separately for every observed FOV. The above set of simultaneous equations were originally solved for the CO_2 amount for each FOV. This is time-consuming procedure, given the large number of FOVs. Instead, we aggregated these data into 1-day, 4° latitude bins before solving for CO_2, which gives essentially identical results.

[33] The highest two latitude time series can contain significant numbers of missing points because of lack of clear FOVs. Figure 4 plots three individual LW time series of observed BTs that illustrate the significant number of missing points at the higher latitudes (54°S is shown). Also shown in the bottom of Figure 4 is the mean Northern Hemisphere BT bias, showing how the observed BTs are getting colder with time, modulated by the seasonal cycle, because of increasing CO_2. The gray curve in the bottom is the associated mean times series of dT_s, which does not exhibit any long-term trend.

[34] The final CO_2 product has dimensions of 30 latitude bins (−60 to +60° latitude in 4° steps) and 1460 days (4 years). Most results shown in this paper use the LW AIRS CO_2 product, which we consider to be more accurate than the SW AIRS CO_2 product. The SW CO_2 product is, however, used for diagnosing errors, especially relative to ECMWF temperature profiles.

3.1. Calibration

[35] The accuracy of a computed radiance is often limited by the accuracy of the molecular spectroscopy used to compute the atmospheric transmission and emission terms in the radiative transfer equation. It is very difficult to get

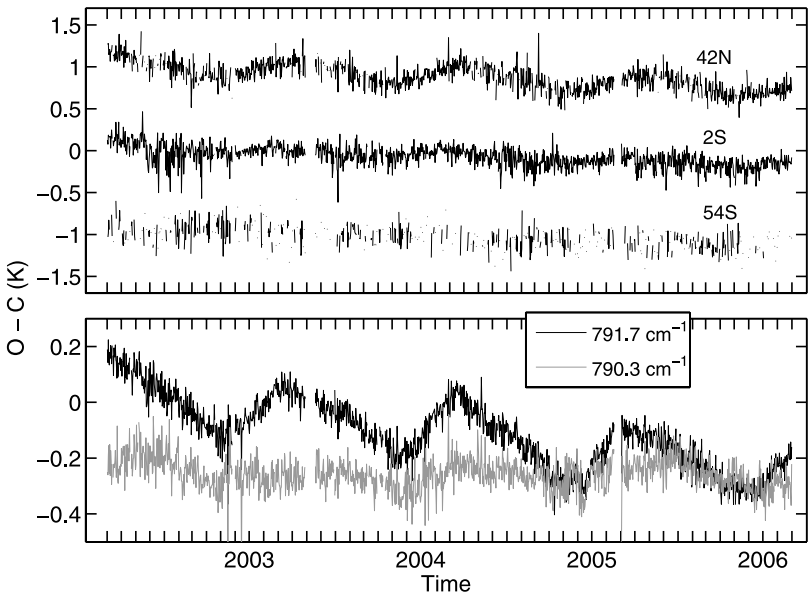

Figure 4. (Top) Examples of 4° latitude binned biases between observed and computed 791.7 cm^{-1} brightness temperatures. The 42N/54S biases have been offset by +1K/−K respectively. (Bottom) Northern Hemisphere mean biases for both the LW CO_2 channel (791.7 cm^{-1}) and the surface channel (790.3 cm^{-1}). Note that, as expected, there is no long-term trend in the surface channel bias. For this plot, and all subsequent plots versus time, tick marks denote the first day of each month, and the year labels are centered below the 1 July tick marks.

agreement among laboratory measurements of molecular vibration-rotation transition strengths, widths, and shapes to even the 2% level. If one takes 2% as the accuracy of the CO_2 optical depths used in the radiative transfer, this translates, for the 791 cm^{-1} CO_2 transition, to an error of 0.22 K in brightness temperature, or an error of about 8 ppm in the CO_2 volume mixing ratio. Given that we expect the AIRS stability to be <0.016 K/year [*Aumann et al.*, 2006], or equivalently <0.5 ppm of CO_2 per year, our measurements will be far more precise than accurate.

[36] The CO_2 record at Mauna Loa provides a very convenient one-time, one-value offset calibration for the AIRS CO_2 measurements. The Mauna Loa CO_2 accuracy is well-established (at the sub-ppm level) and is commonly used as a baseline for comparisons among other measurements. Mauna Loa is particularly suited for the AIRS CO_2 calibration since it is located at ~650 mbar, close to the nominal 550 mbar peak of our CO_2 sensitivity function. In addition, at the latitude of Mauna Loa (19.5°N) atmospheric CO_2 is relatively well mixed, especially compared to other latitudes. We therefore offset our 4-year record of CO_2 to agree with the mean of the Mauna Loa CO_2 values, using our zonal CO_2 values within 8° latitude of Mauna Loa, and only observations in the Pacific Ocean.

[37] This calibration may take into account factors other than CO_2 spectroscopy errors, which could include AIRS radiometric calibration errors and errors in our radiative transfer model separate from transmittance errors. In addition, this one-time calibration adjusts our vertically-averaged CO_2 amount into a nominal 650 mbar value. Between ±60° latitude the peak of the 791 cm^{-1} CO_2 Jacobian only varies by about 50 mbar. The 2400 cm^{-1} kernel function peaks at a slightly lower altitude than the 791 cm^{-1} channel, around 600 mbar.

[38] This calibration led us to increase the AIRS-derived CO_2 amounts by +7.2 ppm for the 791.7 cm^{-1} transition and +9.5 ppm for the 2400 cm^{-1} SW region CO_2 measurement. These values are well within expected spectroscopic and radiometric error budgets. For example, the HITRAN database [*Rothman et al.*, 2005] uncertainty estimate for the 791.7 cm^{-1} CO_2 Q-branch line strengths is 2–5%, which translates into an uncertainty in the CO_2 amount of 8–18 ppm. Note that in the 2400 cm^{-1} region the AIRS radiative transfer model transmittances were previously adjusted, on the basis of coincident radiosonde measurements [see Figure 9 of *Strow et al.*, 2006], and therefore the 9.5 ppm calibration offset derived for the SW CO_2 retrieval cannot be interpreted as the true spectroscopy error.

[39] The AIRS pre-launch radiometric calibration uncertainty was ~0.1 K near 790 cm^{-1} [*Pagano et al.*, 2003], which has been validated in orbit to less than 0.2 K [*Aumann et al.*, 2006]. The 791.7 cm^{-1} channel sensitivity to CO_2 is 0.03 K/ppm, which translates to a minimum uncertainty in CO_2 because of radiometric error of ~3–7 ppm (for a 0.1–0.2 K radiometric uncertainty) that may occur in addition to spectroscopic errors.

[40] All of these considerations suggest that these small calibration adjustments of +7.2 ppm for the LW, and +9.5 ppm for the SW are well within the bounds of our estimated absolute errors.

[41] Figure 5 shows our smoothed zonally averaged CO_2 values for the first four years of AIRS operations averaged over the 19.5 ± 4° latitude range, with and without the +7.2 ppm calibration offset. The bottom shows the difference between the Mauna Loa and AIRS CO_2 as a function of time. Note that the AIRS CO_2 is zonally averaged over the Pacific Ocean while the Mauna

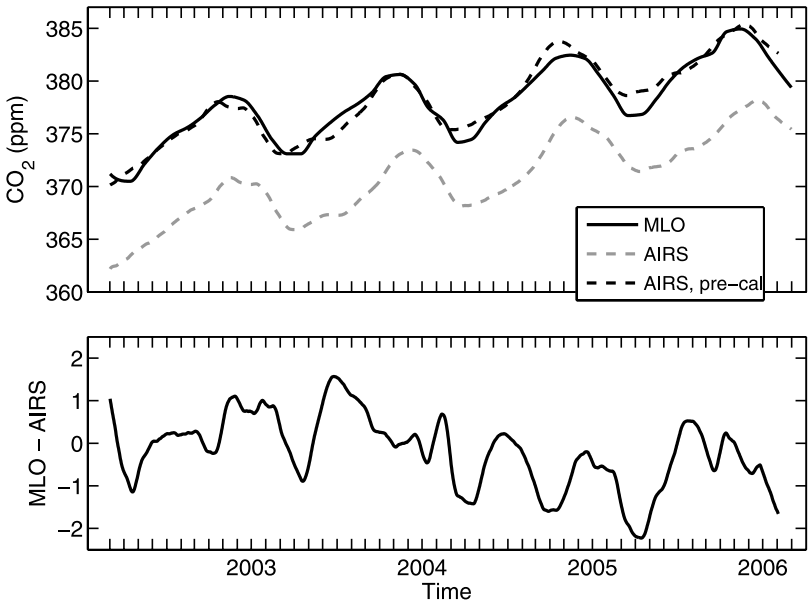

Figure 5. (Top) The NOAA-ESRL GLOBALVIEW CO_2 record at Mauna Loa and the AIRS (LW) derived CO_2 record (Pacific Ocean only) before and after calibration adjustment to the Mauna Loa amount. (Bottom) Mauna Loa minus AIRS CO_2 (after CO_2 offset adjustment).

Loa data is a point measurement, so some disagreement is expected because of the zonal variability observed by AIRS.

[42] For plotting purposes, both in this figure and subsequent figures, we smooth and fill missing data in the CO_2 time series using the Singular Spectrum Analysis (SSA) approach [*Ghil et al.*, 2002; *Kondrashov and Ghil*, 2006]. Only the ±56 and ±60° latitude CO_2 time series needed significant filling. A correlation length of 1 year was used to fill missing points [*Kondrashov and Ghil*, 2006]. For smoothing, we used a correlation length of 40 days, which does not necessarily remove behavior over a shorter time period. We do not use these smoothed results in our main analysis of the CO_2 time series (fits to equation (3)), but instead fit to the original un-smoothed, un-filled CO_2 time series.

[43] The gray dashed curve in the top of Figure 5 is the raw AIRS CO_2 at the Mauna Loa site. A least-squares fit of both of these time series (see section 5.3 for details) indicates that the Mauna Loa seasonal cycle is leading the AIRS seasonal cycle by 28 days. We increased the AIRS phase by this amount, and added in the 7.2 ppm calibration offset, before computing the Mauna Loa minus AIRS curve shown in the bottom.

[44] The Mauna Loa minus AIRS time series has repeated minima in the fall of each year, approximately 3–4 weeks after the Northern Hemisphere boundary layer CO_2 begins rising after the summer draw-down. AIRS may be detecting slightly higher CO_2 amounts than Mauna Loa, since the AIRS zonal average contains scenes closer to continents. The additional minimum in MLO minus AIRS in late winter of 2005 may be related to the slow growth in the boundary layer compared to the AIRS measurements that are discussed in more detail in section 5.3 (see Figure 21).

[45] Since the peak disagreements between Mauna Loa and AIRS are generally <1 ppm in Figure 5, we estimate the accuracy of this calibration to be in the 1 ppm range. A more detailed analysis of the accuracy of the our derived CO_2 product, using other data sources, is given in section 4.

3.2. LW Versus SW CO_2

[46] Comparisons between our AIRS LW and SW CO_2 climatology provides some degree of validation, since these two spectral regions are far apart and are subject to different kinds of interfering processes. For example, the 791 cm^{-1} brightness temperatures can be depressed below the sea surface temperature by up to 7 K in the tropics because of the water vapor continuum, while the max depression in the SW channels due to water vapor is below 1 K. The channel used to derive the surface temperature × emissivity product in the LW has effectively no CO_2 absorption. In the SW all channels used to determine the surface emission have significant CO_2 absorption. Although the 791.7 cm^{-1} channel is less temperature sensitive than the SW channels, it is potentially more sensitive to cloud contamination because of the wavelength sensitivity of the Planck function.

[47] The differential sensitivity of the SW and LW CO_2 to ECMWF model fields is illustrated in Figure 6, where we plot our mean Northern Hemisphere CO_2 climatology derived from both channels sets. We removed a slight bias of 0.25 K between the SW and LW CO_2 for the time period up to 1 February 2006 in order to highlight the change in the CO_2 values after this time. The bottom of this plot shows the smoothed difference between these two time-series, which clearly highlights a sharp change of ~2–3 ppm in February 2006 that we trace to changes in the ECMWF model (see http://www.ecmwf.int/products/data/operational_system/evolution/evolution_2006.html#1February2006). The sensitivity calculations plotted in Figure 2 are for a U.S. standard atmosphere and show that the LW CO_2 retrieval is about four times less sensitive to ECMWF than the SW results. More detailed calculations show that this ratio is ~2.6 at the equator and grows to ~4.9 at the higher latitudes.

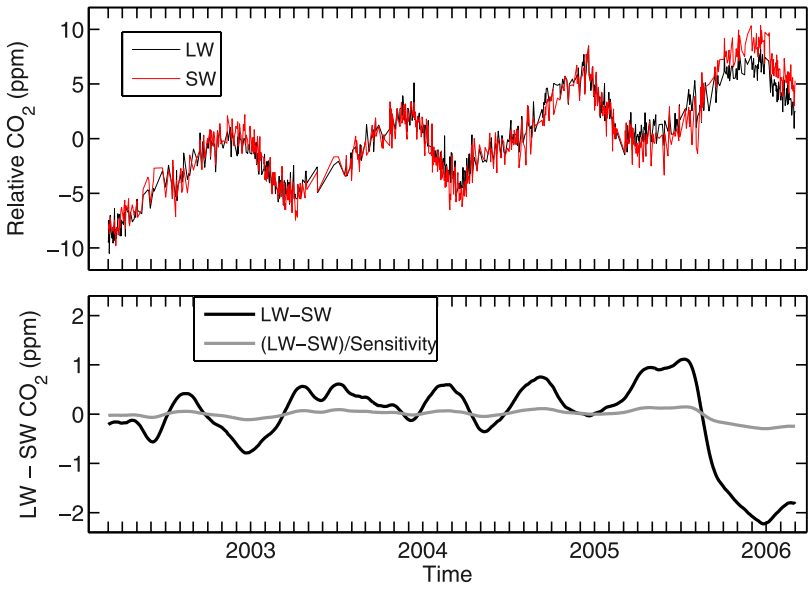

Figure 6. (Top) LW and SW AIRS CO_2, 5° to 45° latitude mean. (Bottom) Smoothed LW minus SW CO_2; the same quantity was divided by the differential sensitivity between LW and SW to temperature profile errors. (The differential sensitivity is the ratio of the channel average of equation (1) evaluated for the SW divided by equation (1) evaluated for the LW CO_2 channel.) The gray curve is an estimate of the uncertainty in our LW AIRS CO_2.

[48] One way to estimate of the effects of ECMWF model error on our LW CO_2 product is to divide the difference between the LW and SW CO_2 by this sensitivity ratio, which is the gray curve in the bottom of Figure 6. While this is probably an underestimate of the impact of ECMWF errors on the LW CO_2, it does suggest that they may be less than 1 ppm. If the ECMWF temperature shift is distributed non-uniformly in the vertical, this error may be larger, since our sensitivity calculations used a vertically constant temperature offset.

[49] A comparison of the 3-year mean of the LW and SW CO_2 versus latitude is shown in Figure 7. The SW CO_2 has been normalized to give the same mean CO_2 as the LW, averaged over latitude. These two curves are similar but do exhibit systematic differences of up to 1 ppm, depending upon latitude. These may occur because the SW CO_2

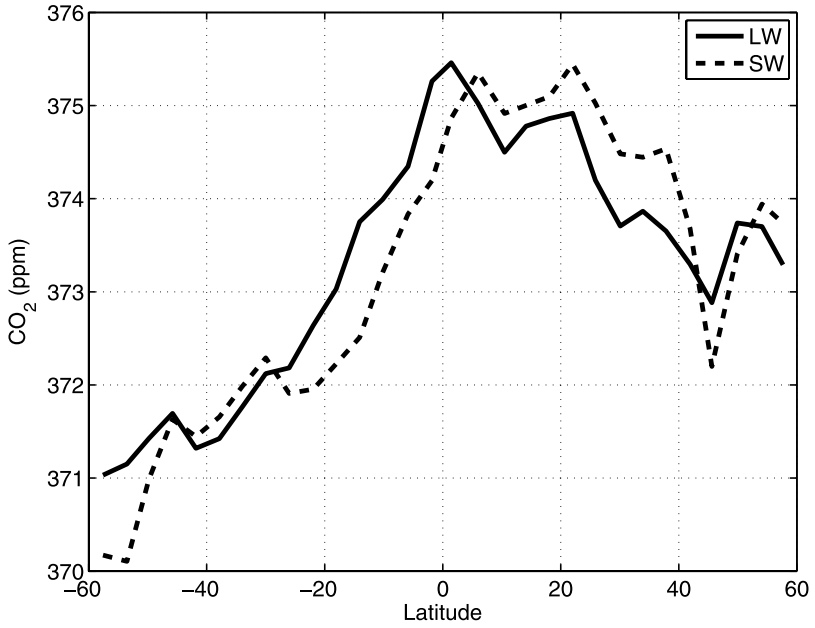

Figure 7. Three-year mean (2003–2005) of detrended AIRS CO_2. The solid line is the results reported here using the LW 791.7 cm^{-1} channel; the dashed line is the AIRS CO_2 derived from the SW 2400 cm^{-1} region, normalized to give the same mean CO_2 as the 791.7 cm^{-1} channel result when averaged over latitude. The error in the LW CO_2 caused by inaccuracies in the ECMWF temperature profiles should be several times smaller than the differences between the LW and SW CO_2 amounts shown here.

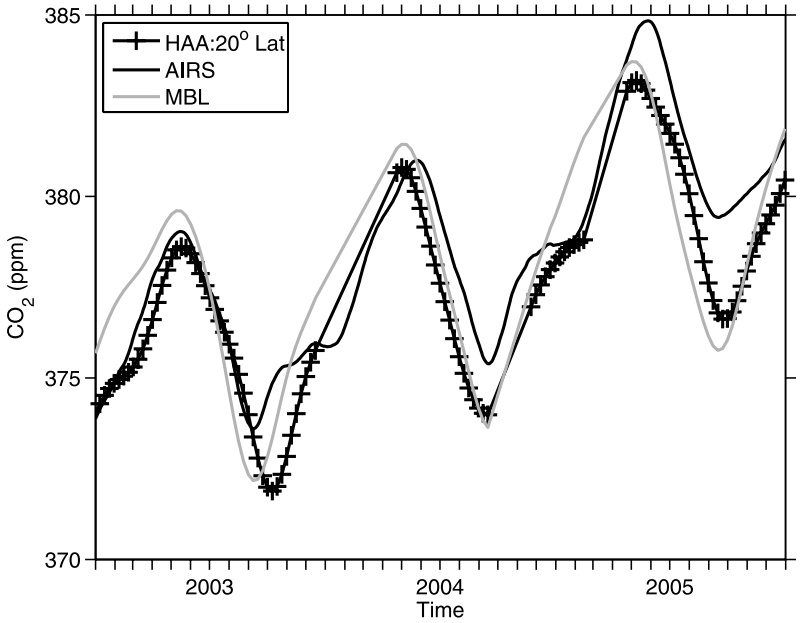

Figure 8. Molokai Island, Hawaii (HAA) CO_2 from aircraft flights at 3.5 km (650 mbar) compared with AIRS (LW) and NOAA-ESRL MBL boundary layer CO_2.

Jacobian is larger at lower altitudes and thus more sensitive to ECMWF temperature profile errors. If there is indeed more CO_2 at higher altitudes in the southern tropics, this would result in a lower SW CO_2 in that region. Conversely, above $\sim 10^\circ$ latitude, the mean CO_2 is higher at low altitudes, making the SW CO_2 somewhat higher then the LW CO_2.

4. Validation

[50] We compare the AIRS zonal CO_2 to the three aircraft flight series in the NOAA/ESRL GLOBALVIEW database that are over open ocean in the $\pm 60^\circ$ latitude range. For two of these flight series, HAA (Molokai Island, Hawaii, $+21.2^\circ$ latitude, -159° longitude) and RTA (Rarotonga, Cook Islands, -21.25° latitude, -160° longitude), we compare to data taken at flight altitudes of 3.5 km ($\sim$650 mbar), close to the altitude of Mauna Loa, which we used for our calibration constant. In addition, we also compare our results to the extensive set of aircraft measurements by *Matsueda et al.* [2002] taken on commercial Japan airlines flights (JAL), at an altitude of 10.5 km ($\sim$250 mbar). The JAL CO_2 measurements are much higher in altitude than the peak of our CO_2 measurement Jacobian, although we still have significant contributions from that altitude (see

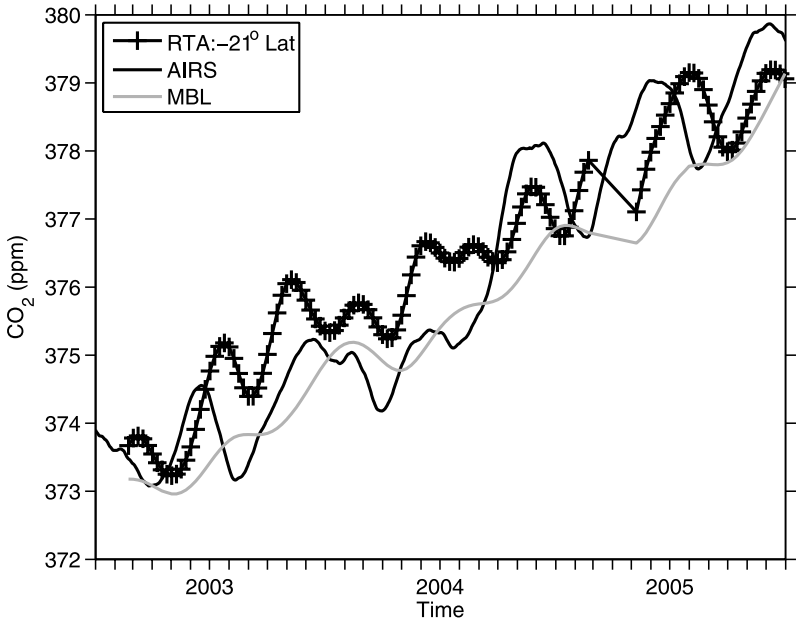

Figure 9. Rarotonga, Cook Islands (RTA) CO_2 from aircraft flights at 3.5 km (650 mbar) compared with AIRS (LW) and NOAA-ESRL MBL boundary layer CO_2.

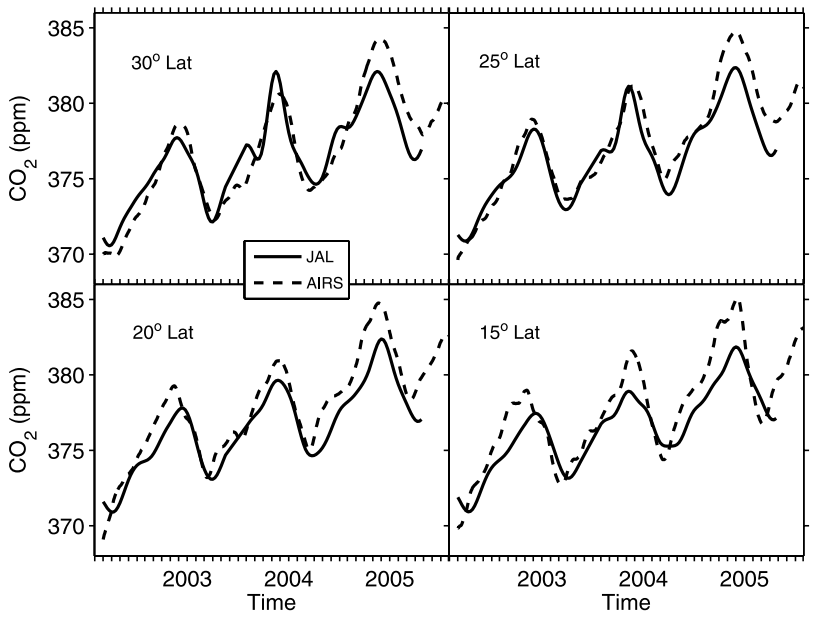

Figure 10. Japan Airlines (JAL) CO_2 measured at 10.5 km (250 mbar) compared with AIRS (LW) for 15° to 30° latitude in 5° increments.

Figure 3). For the lower altitude HAA and RTA data we also plot the NOAA GLOBALVIEW MBL values for reference.

[51] Figure 8 shows that the AIRS, HAA, and MBL time series have considerable overlap over the three years shown. Not surprisingly, HAA versus AIRS exhibits similarities to the comparison of Mauna Loa versus AIRS. For example, the AIRS zonal average is again slightly higher than HAA 3–4 weeks after the Northern Hemisphere boundary layer CO_2 begins rising after the summer draw-down. (Note that this feature cannot be seen in 2004 since HAA had a data gap during that fall.) This feature may be due to the influence of the Indian/Arabian ocean CO_2 on the AIRS zonal CO_2 measurement (see section 5 for a more detailed discussion).

[52] HAA minus AIRS is −0.71 ppm on average, with a standard deviation of 0.86 ppm. These statistical comparisons combine the AIRS CO_2 uncertainty and the zonal variability that is folded into the AIRS CO_2 product. Generally the MBL ramp-up of CO_2 in the winter is stronger than either the HAA or AIRS behavior (presumably because of decreased convection to higher altitudes) while both HAA and AIRS CO_2 values follow the draw-down of CO_2 more closely during the middle of the year (increased convection).

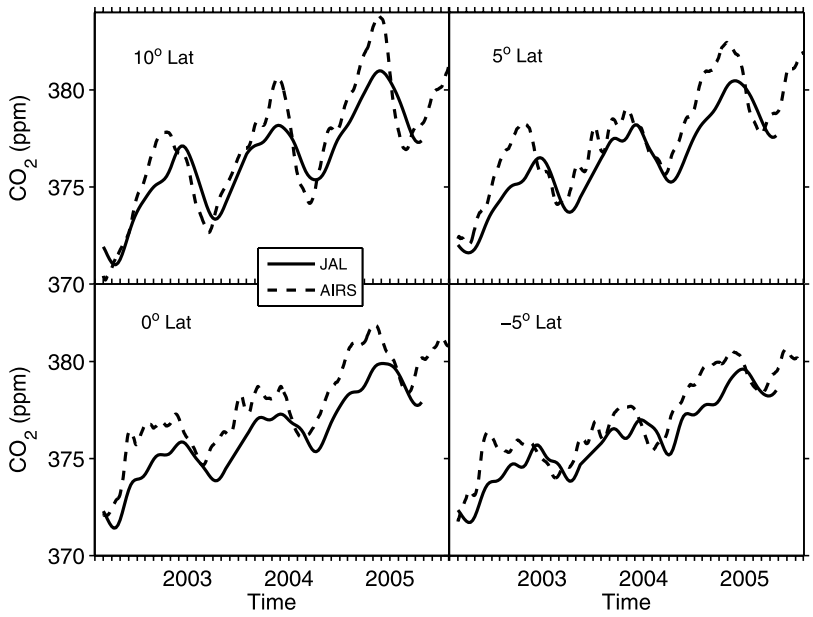

Figure 11. JAL CO_2 measured at 10.5 km (250 mbar) compared with AIRS (LW) for −5° to +10° latitude in 5° increments.

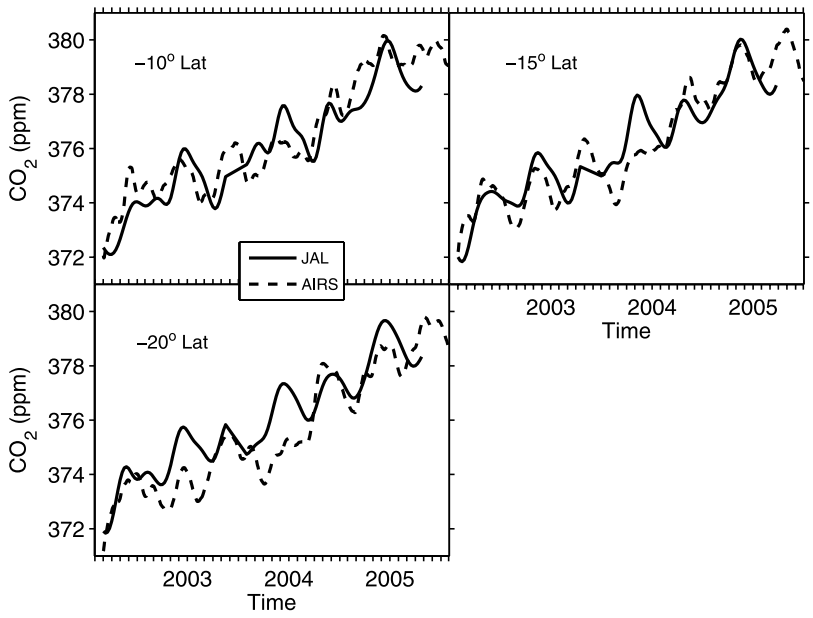

Figure 12. JAL CO_2 measured at 10.5 km (250 mbar) compared with AIRS (LW) for $-10°$ to $-20°$ latitude in 5° increments.

[53] The Rarotonga flights provide a southern hemisphere validation at $-21°$ latitude, shown in Figure 9. Since there is little seasonal variation of CO_2 in the southern hemisphere, this figure highlights the CO_2 growth rate. Note that the y-scale in this figure only spans ~8 ppm compared to ~15 ppm in Figure 8. The RTA CO_2 is higher than the MBL reference matrix, not unexpected due enhanced mid-tropospheric interhemispherical transport compared to the boundary layer, [see *Strahan et al.*, 1998, Figure 6]. On average, the RTA values are 0.78 ppm higher than AIRS with a standard deviation of 0.89 ppm.

[54] Figures 10, 11, and 12 compare the 250 mbar JAL CO_2 time series to our AIRS zonal CO_2 from +30 to $-20°$ latitude in 5-degree increments. The JAL flights are over open ocean, with little nearby continental influence, especially at these altitudes. The +30° to +15° latitude graphs show very similar amplitudes and phases for the seasonal cycles of AIRS and JAL. There are differences of up to 2 ppm

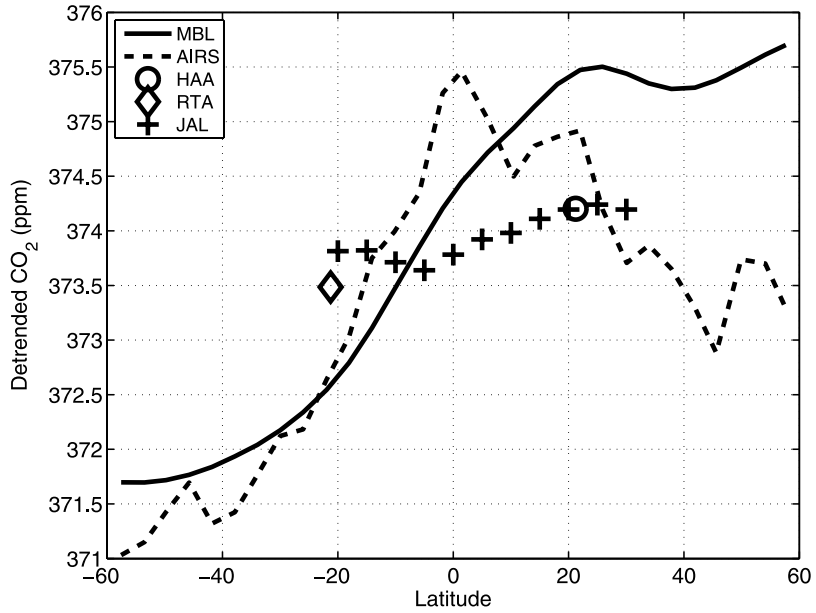

Figure 13. Three-year mean of detrended CO_2 from AIRS (LW) compared with (1) NOAA-ESRL marine boundary layer (MBL) climatology, (2) Molokai Island, Hawaii (HHA) aircraft measurements at 3.5 km (650 mbar), (3) Rarotonga, Cook Islands (RTA) aircraft measurements at 3.5 km (650 mbar), and (4) Japan Airlines (JAL) 10.5 km (250 mbar) measurements. All values are adjusted to a reference time of 1 January 2003.

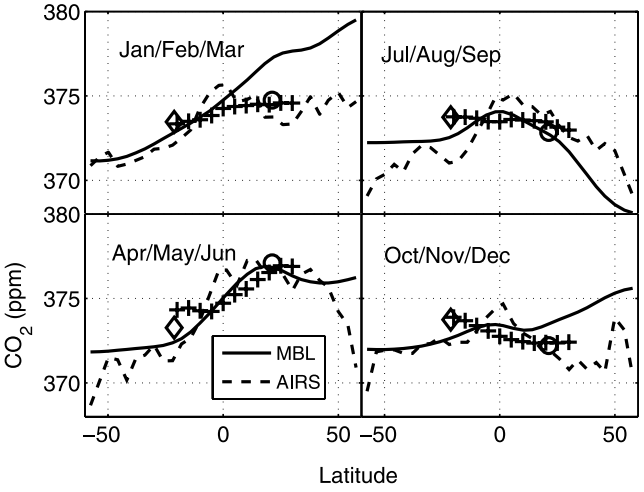

Figure 14. Same data and symbols as in Figure 13 but separated by season.

at these latitudes (early summer 2004/2005 for +30° latitude, for example). In addition, the AIRS CO_2 is slightly higher during 2005. As you move to lower latitudes, the amplitude of the JAL seasonal cycle becomes smaller than the AIRS seasonal cycle. This reduction of the JAL seasonal cycle is most pronounced in Figure 11 for the +10° and +5° latitude data, where the AIRS seasonal cycle starts to lead the JAL cycle. Once you approach the equator, the shapes of the JAL and AIRS seasonal cycles become very similar, with just small phase differences. Below −10° latitude, there are only small oscillations about the overall growth curve of CO_2 for both AIRS and JAL, with no strong correlation other than the yearly growth rate.

[55] Figures 13 and 14 summarize these validation comparisons, and include the MBL climatology for reference. In Figure 13 we detrended and deseasonalized the aircraft time series by fitting them to the following relation,

$$CO_2(t) = C + Rate \times t + \sum_{i=1}^{4} [a_i \sin(2\pi i t + \phi_i)] \qquad (3)$$

where C is a constant, *Rate* is the linear growth rate of CO_2, a_i are the amplitudes of the seasonal cycle and the next three harmonics, and ϕ_i are the phases of the seasonal cycle and harmonics. The aircraft points in Figure 13 are $C + Rate \times (t_r - t_o)$ where t_o is the starting time of the aircraft time series, which we set as September 2002 or whenever the aircraft data start after this date. Our reference time is the start of 2003, so t_r = 2003. This approach helps remove artifacts due to missing data, although it does suppress any anomalies in these time series, but they are very small.

[56] The AIRS and MBL data are treated slightly differently, since they are basically continuous. For these data we instead construct $CO_2(t) - Rate \times (t - t_r)$ separately for the three years t = 2003–2005. We then plot the average CO_2 for these three years. This approach leaves any anomalies in the average CO_2, although we find that this only changes the mean (over latitude) CO_2 values by 0.13 ± 0.15 ppm if we instead had plotted the same quantity as for the aircraft data.

[57] Figure 13 clearly shows that the rectifier effect in the Northern Hemisphere produces a mid-troposphere to boundary layer CO_2 gradient above 20° latitude that grows to ~2 ppm at +60° latitude. In the Southern Hemisphere the AIRS CO_2 generally agrees with MBL to within 1 ppm, with AIRS higher in the tropics and lower in the southern mid-latitudes.

[58] The standard deviations (over time) between the two 3.5 km aircraft flights and the AIRS zonal CO_2 were 0.86, 0.89 ppm respectively for the HAA and RTA sites. Although the JAL flights were at significantly higher altitudes (10 km) the average standard deviation (over time) for the 11 latitudes included in GLOBALVIEW was 1.0 ppm. We did not adjust the AIRS seasonal phase to the in situ CO_2 seasonal phase in computing these standard deviations since it can introduce significant errors at latitudes with small seasonal cycles. For the JAL flights, two latitudes with a seasonal cycle phase almost equal to the AIRS observed phase (20° and 25° latitude) have a standard deviation of 0.9 ppm for all observations, 1.0 ppm for Pacific observations only. Again, these types of comparisons will contain zonal variability, possibly limiting their statistical meaning.

[59] A common way to examine CO_2 variability is to examine the latitudinal dependence by season, as in Figure 14, using the same data processing approach used for Figure 13. In January–March the boundary layer CO_2 is continuing its climb that started in the Fall, but transport to higher altitudes is limited so the AIRS values fall well below the boundary layer values. By April–June the boundary layer has begun to draw down, and the CO_2 profile becomes relatively constant. During the continued draw down in the summer months the Northern Hemisphere boundary layer values drop below the AIRS CO_2 amounts, until the late fall when the boundary layer CO_2 starts to increase again and becomes higher than the AIRS mid- to lower-tropospheric CO_2. In general, the JAL and HAA Northern Hemisphere CO_2 values closely follow the AIRS values over time, although the AIRS CO_2 has a persistent higher value near the equator.

[60] We conclude that the AIRS CO_2 climatology accuracy is approaching the 0.5–1.0 ppm level, at least in the −20° to +30° latitude range where validation data exists. In the southern hemisphere, from −20° to −60° latitude, we have no in situ mid-tropospheric CO_2 data over ocean, and there is always the question if the Northern Hemisphere and tropical ECMWF statistical accuracy we depend upon holds in these lower latitudes.

[61] Finally, we note that close to the equator that the AIRS CO_2 is higher than both the MBL and JAL values. This could be true because of the preferential transport to higher altitudes sensed by the JAL flights, but it could also be due to undetected clouds in the fields of view. This persistent high CO_2 amount does not appear to have a clear seasonal component, suggesting it might not be a cloud effect. Further analysis is needed to completely evaluate these very small deviations that are in the <1 ppm range.

5. Results

[62] Figure 15, top panel, is the main result of this paper, 4 years of zonally averaged CO_2 concentrations at a nominal pressure of 600 mbar. Three features are apparent; (1) the CO_2 concentrations are growing in time, (2) there is a strong seasonal CO_2 cycle in the Northern Hemisphere, and (3) there exists a much weaker seasonal cycle in parts of

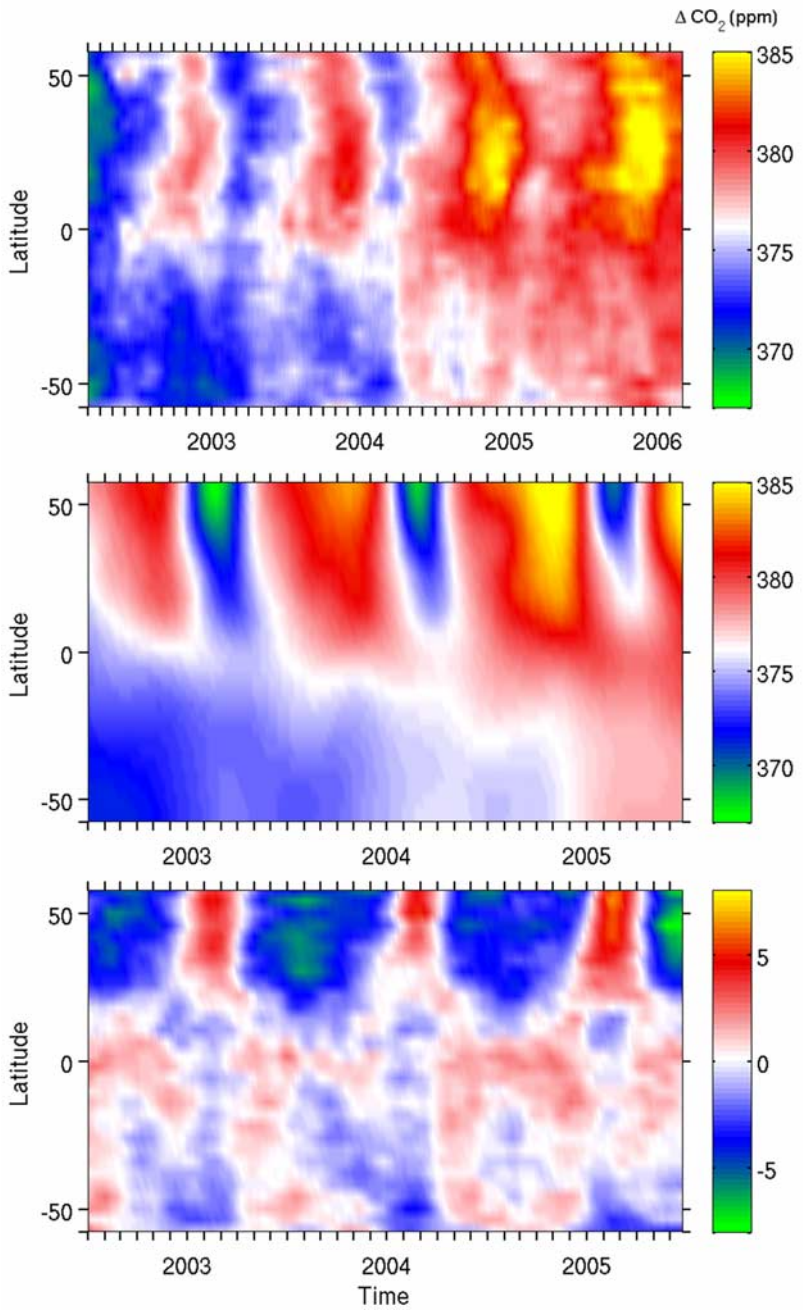

Figure 15. (Top) AIRS retrieved CO_2 using LW channels over the first 4 years of operation. (Middle) NOAA-ESRL MBL CO_2 product for years 2003–2006. (Bottom) AIRS minus MBL CO_2 for years 2003–2006. The AIRS CO_2 nominal peak sensitivity is at 600 mbar, while the MBL CO_2 applies to the marine boundary layer.

the southern hemisphere. CO_2 values vary from a minimum of ~367 ppm to a maximum of ~385, a range of 18 ppm.

[63] Comparisons of our derived zonal CO_2 climatology to the NOAA/ESRL GLOBALVIEW Marine Boundary Layer (MBL) reference matrix provide some level of validation as well as highlighting the differences between our nominal 5 km altitude measurements versus the MBL boundary layer smooth zonal climatology. Figure 15, middle, shows the GLOBALVIEW MBL CO_2 using the same CO_2 scale as in the top, while the AIRS minus MBL difference is shown in the bottom. Note that only 3 years of MBL CO_2 data is shown since the MBL CO_2 for 2006 was not yet available during this study.

[64] As expected, comparisons of the AIRS to MBL CO_2 shows the strong seasonal rectifier effect [*Denning et al.*, 1996] in the Northern Hemisphere, where the min/max values of the mid-tropospheric seasonal cycle are lower than the boundary layers excursions. The CO_2 rectifier is due to the time covariance between the CO_2 surface fluxes and atmospheric transport. For example, in the late autumn when CO_2 is increasing in the boundary layer, weak, infrequent convection minimizes transport of the seasonally

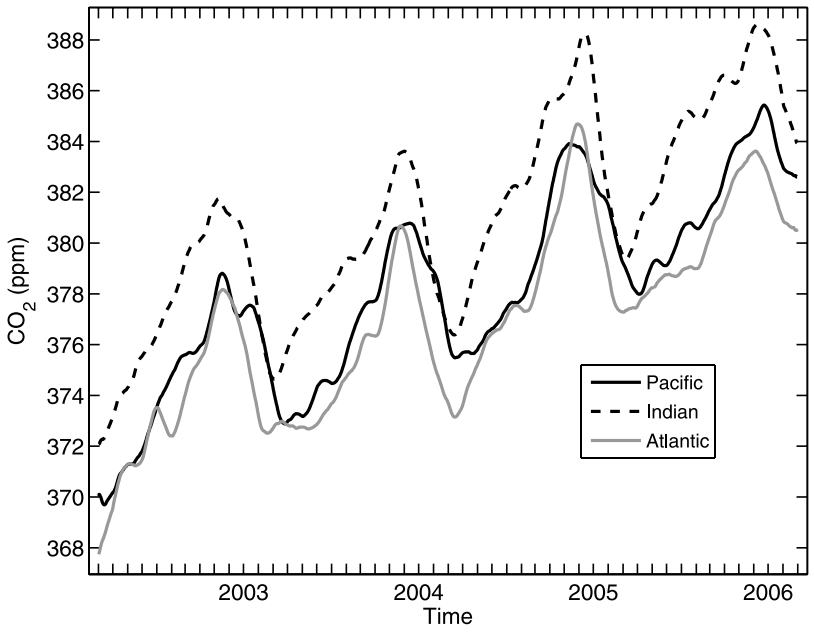

Figure 16. Smoothed CO_2 (LW channels) separated by ocean, averaged over 14°–22° latitude range. Higher CO_2 values in the Indian Ocean are presumably because of transport of nearby Asian continental air.

high CO_2 to the mid-troposphere. Conversely, in the summer months, the boundary layer CO_2 is low due photosynthesis, and increased convection transports these lower CO_2 values to the free troposphere. These so-called rectifier effects lead to accumulation of CO_2 near the ground with depletion aloft in the Northern Hemisphere.

[65] In the southern hemisphere there is evidence for a seasonal cycle nearly 180° out-of-phase with the Northern Hemisphere cycle, but the time series is relatively noisy. The difference between AIRS and MBL appears to have an anomaly in mid-2005, which will be considered in more detail in section 5.3.

[66] One interesting difference between these two climatologies is seen in the +20 to −10° latitude range in the July time frame. The AIRS CO_2 decreases rather quickly from +20° to −10° latitude, while the MBL CO_2 has a much lower negative slope. The color scale in Figure 15 makes this effect easiest to observe for July 2003. This observation is also evident in our phase analysis of the AIRS and MBL seasonal cycle and is presented in more detail in section 5.1,

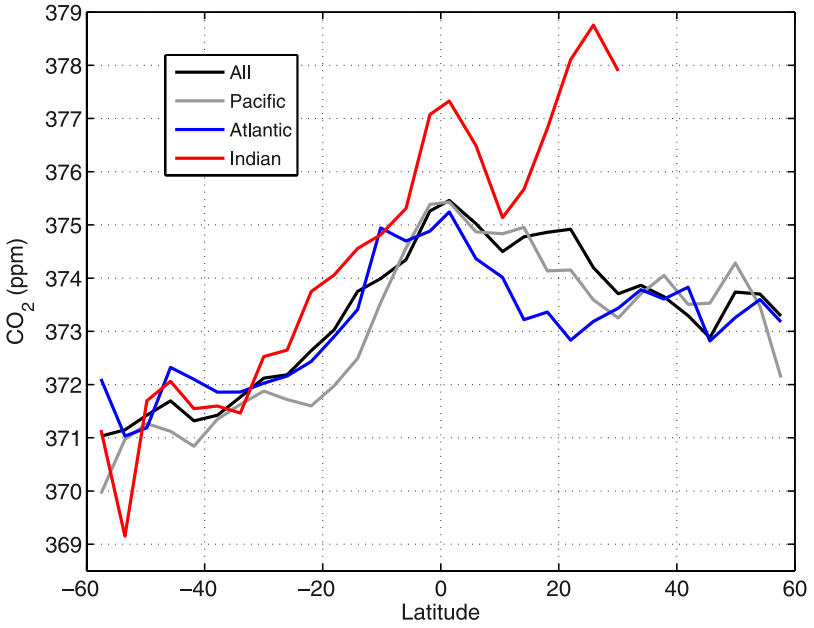

Figure 17. Four-year mean CO_2 from AIRS (LW channels), separated by ocean, plus mean over all oceans. Higher CO_2 values in the northern latitudes of the Indian Ocean are indicative of transport of nearby CO_2-rich Asian continental air.

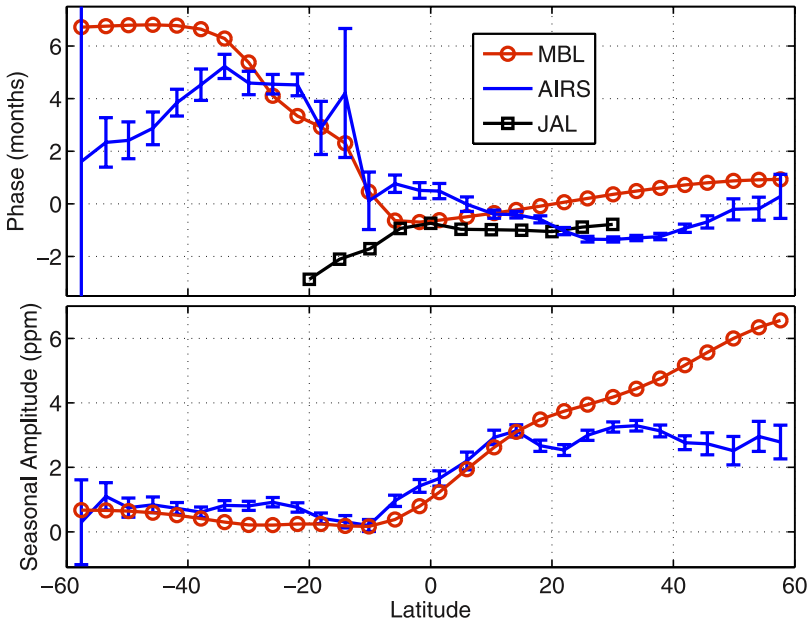

Figure 18. (Top) Phase of the CO_2 seasonal cycle (fundamental mode) for AIRS (LW), NOAA-ESRL MBL, and JAL. Phase is given in months; 2π phase = 12 months. (Bottom) Amplitude of the CO_2 seasonal cycle (fundamental mode) for AIRS (LW) and MBL. Errors bars shown for AIRS in both are 95% confidence intervals.

where we find that the AIRS CO_2 cycle leads the MBL cycle between $+10^\circ$ to -10° latitude. In the higher latitudes the MBL phase leads the AIRS phase because of the time delay in the response of the atmosphere to the surface CO_2 forcing function. We conjecture that this relative phase reversal in the tropics is due to transport of higher latitude, more CO_2 poor air masses, to the tropics during this time frame.

[67] Figure 16 shows our LW 4-year time series of CO_2 averaged from $14-22^\circ$ latitude, separated by ocean. For the Indian ocean this latitude range samples very close to the Asian continent and indeed shows significantly higher CO_2 amounts than the mean CO_2 for the same latitude range for either the Pacific or Atlantic oceans. In Figure 17 we have averaged these CO_2 time series over all four years and plotted the means versus latitude. This plot clearly shows that the Indian Ocean CO_2 values are about 1–4 ppm higher near the continental boundary than in the Atlantic or Pacific. These differences drop sharply as you move to the open Indian ocean at the lower latitudes, where the continental influence has lessened.

[68] We now examine the seasonal cycles of our CO_2 climatology in more detail, mostly relative to NOAA-ESRL's smoothed boundary layer product, MBL. The seasonal amplitudes and phases presented here are derived from least-squares fits of the raw AIRS CO_2 data, and the MBL time series, to equation (3). The following sections discusses the phase of the fundamental seasonal cycle, ϕ_1, followed by a discussion of its amplitude, a_1.

5.1. Seasonal Cycle Phases

[69] The relative phase between the MBL and AIRS CO_2 shown in Figure 18, top, exhibits some interesting behaviors, most likely related to transport. We have plotted the phase in units of months, where 12 months = 2π in phase. Also shown are the 95% confidence limits from the fits for the AIRS CO_2 seasonal phase.

[70] Phase plots such as these may potentially prove useful for comparisons between transport models and satellite data. This figure should be viewed in parallel with bottom of Figure 18, which shows the amplitude of the seasonal cycle versus latitude.

[71] First we note that the MBL indeed leads the mid-tropospheric AIRS CO_2 in the higher northern latitudes as it takes time for the boundary layer cycle to propagate into the mid-troposphere. However, in the deep tropics the AIRS CO_2 leads MBL between $\pm 10^\circ$. As you move south, the AIRS and MBL phases are similar until -30° latitude where the MBL phase becomes 180° out-of-phase with it's northern latitude values, while the AIRS phase starts decreasing as you move south.

[72] The error bars reflect several mechanisms. From $+50^\circ$ to $+60^\circ$ latitude, the error bars are rather large because of the sparsity of data, which introduces both noise, and missing data, into the high-latitude record. In the mid-latitudes the phase error bars are quite small, because the data density increases and the seasonal cycle is quite large. The error bars then increase as you move south mostly because the amplitude of the seasonal cycle is decreasing. Below -10° latitude the retrieved amplitude of seasonal cycle is less than 1 ppm, causing much larger error bars, especially between -10° to -20° latitude. It may also be the case that a harmonic analysis is not the most appropriate way to understand the CO_2 time variability in this latitude region. However, the phase curve is relatively smooth in this region given such small seasonal amplitudes, and it generally follows the MBL phase curve, until -30° latitude where the MBL curve moves steadily higher to reach a level this is 180° out of phase with the northern latitude MBL phase.

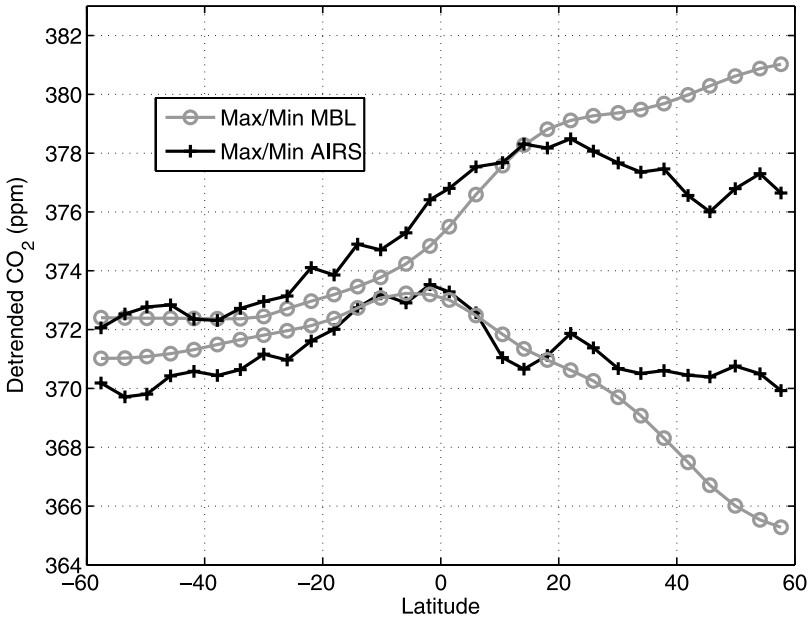

Figure 19. Maxima and minima of the amplitudes of the 3-year detrended AIRS (LW) and NOAA-ESRL MBL time series as a function of latitude. See the text for a possible explanation for the dip in the AIRS minimum CO_2 in the +10° to +20° latitudes.

[73] Below −30° latitude the AIRS CO_2 phase steadily decreases relative to the MBL phase. The error bars increase again as you move south, mostly because of lowered observations statistics. Because the seasonal amplitude is so small in the southern hemisphere, and because there is more uncertainty in the ECMWF model data, the southern hemisphere phase results may be an artifact of our measurement approach, and must be considered with caution. However, it is encouraging that the MBL and AIRS CO_2 phases agree in the −10° to −30° latitudes. Also note that CO_2 may exhibit a 2π phase change slightly below the equator that we cannot detect with these data.

[74] Probably the most interesting phase result is the increase in phase of the AIRS CO_2 relative to MBL between ±10°. At +10° latitude the AIRS CO_2 starts to lead MBL, reaching a maximum lead of almost $1\frac{1}{2}$ months near −5°. Note that at +10°, where the AIRS and MBL phases cross, we also see that the AIRS and MBL seasonal amplitudes become identical, although the mean value (over time) of AIRS is still about 1 ppm lower. This increase in the AIRS CO_2 phase in the deep tropics is likely due to meridional transport from higher latitudes [*Nakazawa et al.*, 1991], especially in the upper tropospheric, which we partially sense with the AIRS CO_2 channels. Note that the AIRS deep tropics CO_2 phase is about the same as the MBL phase at +30°.

5.2. Seasonal Cycle Amplitudes

[75] Figure 18, bottom, shows that the AIRS CO_2 seasonal cycle has an almost constant amplitude from +60° to ∼+10° latitude. Also plotted are the 95% confidence limits for the fitted amplitudes. Below 10°, down to out lowest measured latitude of −60° latitude there is very little difference between the AIRS and MBL CO_2 amplitudes. There is some evidence in the −20° to −40° latitude region that the AIRS mid-tropospheric season cycle is larger than MBL, but the differences are small. This could be due to upper and middle tropospheric interhemispherical transport, which is expected to be larger than in the boundary layer [*Nakazawa et al.*, 1991; *Strahan et al.*, 1998].

[76] The JAL, HAA, and RTA seasonal amplitudes are also plotted in Figure 18, bottom. Both the HAA and RTA amplitudes are very similar to the AIRS CO_2 amplitude, as would be expected, although the RTA amplitude is closer to the MBL amplitude than AIRS.

[77] Since the JAL CO_2 measurements are taken at 250 mbar, well above the ∼550 mbar peak of the AIRS CO_2 sensitivity, we do not expect the amplitudes to be identical. In general one would expect the JAL amplitude to be smaller than both MBL and AIRS in the northern latitudes since it is more distant from the CO_2 forcing function. However, from −10° to −15° latitude the JAL amplitude is considerably higher than either AIRS or MBL, neither of which show significant seasonal variability. This is also consistent with enhanced meridional transport from the Northern Hemisphere at higher altitudes [see *Strahan et al.*, 1998, Figure 6].

[78] Between −20° and −40° latitude the amplitude of the AIRS seasonal cycle is almost 1 ppm, compared to the MBL seasonal cycle amplitude of close to zero. This result would again suggest that meridional transport of air from the Northern Hemisphere may be dominating the CO_2 cycle in the nominal 300−800 mbar region sensed by our AIRS measurement. No JAL data exists for comparison between −20° and −40° latitudes.

[79] Figure 19 is another view of the AIRS and MBL seasonal amplitude, except here we plot the maximum and minimum of the seasonal cycle over the whole year. This view of the data highlights differences between MBL and AIRS during the draw-down of CO_2 versus the build-up of CO_2. Note that the rectifier effect is very symmetric at the highest latitudes. As you move south, it appears that during

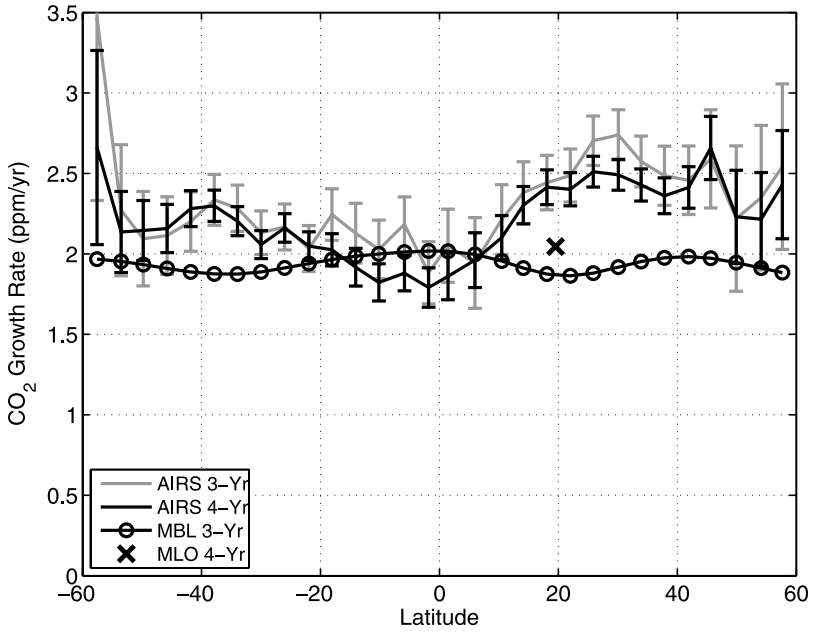

Figure 20. CO_2 growth rates for the full 4-year AIRS record, for the 2003–2005 3-year AIRS record (both using LW channels), and for the same 2003–2005 3-year record from the NOAA-ESRL MBL climatology. Also shown in the Mauna Loa is the growth rate for the same time period as the AIRS 4-year CO_2 record. Error bars shown for the AIRS measurements are 95% confidence intervals.

CO_2 draw-down (minimum) the AIRS mid-tropospheric CO_2 reaches or goes slightly below the MBL minimum from +10 to +20°. This may be caused by the fact that the sharp Northern Hemisphere draw-down of CO_2 begins in May when convection is increasing. CO_2 transport from higher latitudes pushes the +10° latitude mid-tropospheric CO_2 downward more quickly than the boundary layer values at +10°, which are also decreasing, but not as quickly. This negative dip in the AIRS CO_2 minimum is what causes the slight increase in the CO_2 seasonal amplitude at this latitude. A corresponding increase in the maximum of the AIRS CO_2 near +10° latitude is not expected since there is less convection in the winter and early spring when the Northern Hemisphere CO_2 is reaching a maximum.

[80] The MBL seasonal oscillation in the southern hemisphere is very small, generally less than 1 ppm. The AIRS-derived maximum CO_2 in this region is very close to the MBL values, while the AIRS minimum values are about 2 ppm lower than the AIRS maximum values. As discussed earlier, these very small differences between AIRS and MBL in the southern hemisphere are difficult to validate, and may be due to errors in either data set. However, they both show similar trends, both with latitude and with the offset between maximum and minimum values.

5.3. CO_2 Growth Rates

[81] The CO_2 growth rates as a function of latitude, fitted using equation (3), are plotting in Figure 20, for (1) the AIRS 4-year CO_2 record, (2) three years of AIRS, 2003–2005, (3) MBL during the same 3-year time span, and (4) the 4-year Mauna Loa rate. Deriving accurate CO_2 growth rate information from AIRS is highly dependent on the stability of both the AIRS radiometry and the ECMWF model. These rates are averages from 1 September 2002 to 30 August 2006 for the 4-year rate, and from 1 January 2003 to 31 December 2005 for the 3-year rates. The AIRS 4-year rates include the February 2006 time period when we observed a change in the ECMWF model that was reflected as an offset of ~3 ppm in the SW versus LW AIRS CO_2 amounts. The 3-year rates do not include the time period of this model change.

[82] The AIRS CO_2 growth rates were derived using the raw daily average CO_2. For the −50° to +50° latitudes, almost all daily bins are populated, allowing a good estimation of the level of autocorrelation in each of the zonally binned time series. We used the lag-1 autocorrelation to determine if the normal least-squares error estimates must be increased to account for non-Gaussian statistics [*Santer et al.*, 2000] and found these corrections to be negligible for the ±40° latitude range where our daily time series is continuous. Consequently, the rate error bars are the standard least-squares 95% confidence intervals.

[83] In general the retrieved rates are quite close to the equivalent MBL rates, with a maximum difference of about 0.5 ppm/year in the 20°–40° latitude range. Note that 0.5 ppm/year is equivalent to only a 0.015 K/year brightness temperature change in the 791.7 cm^{-1} channel. The AIRS CO_2 rates are about 0.5 ppm/year higher for +20° latitude and beyond, and about 0.25 ppm/year higher in the southern mid-latitudes, from ~−20° to −55° latitude. Our error bars grow rapidly as you approach ±60° latitude because of far fewer clear FOVs in our data set, with many days missing, especially in the winter. In the tropics from ~+10 to −20° latitude the AIRS and MBL rates agree within the AIRS error bars.

[84] Table 1 summarizes the rates measurements and comparison to other sources. If one averages over all latitudes, the AIRS 4-year rate is 2.21 ppm/year with a standard deviation of ±0.24 ppm/year (standard deviation is over

Table 1. Growth Rates From Various Data Sets[a]

Time Series	Rate/Std, ppm/yr
AIRS 4 yr	2.21 ± 0.24
AIRS 3 yr	2.32 ± 0.31
MBL 3 yr	1.94 ± 0.05
MLO 4 yr	2.05
AIRS 20–40° subset	(1.86, 2.56) = 2.21
MBL 20–40° subset	(2.07, 2.88) = 2.48

[a]The AIRS growth rates all use the LW CO_2. Standard deviations are taken over latitudes. Rates averaged from only 20° to 40° latitude are only for two particular time period subsets that are noted in the text and in the Figure 21 caption.

latitude). The AIRS 3-year rate is 2.32 ± 0.31 ppm/year. This compares to the mean MBL rate of 1.94 ppm/year (3-year rate). The difference between the AIRS and MBL 3-year rates is 0.38 ppm/year, which is equivalent to a brightness temperature change of 0.011 K/year. The MLO 4-year rate differs from the latitudinally averaged AIRS 4-year rate by 0.16 ppm/year, or a brightness temperature difference of 0.0048 K/year. If you just compare the AIRS 4-year rate at the MLO latitude, to the MLO 4-year rate, you get a difference of 0.36 ppm/year or 0.011 K/year in brightness temperature. These results suggest that the AIRS CO_2 growth rates are accurate to at least 0.4 ppm/year, and possibly better.

[85] Some insight into the differences between the AIRS versus MBL rates is gained by plotting the deseasonalized time-series. Figure 21 is a graph of

$$CO_2(t) - C - \sum_{i=1}^{4} [a_i \sin(2\pi i t + \phi_i)] \quad (4)$$

which subtracts the fitted offset constant and sinusoidal terms from the raw CO_2 time series. We chose to plot the mean of this series between 20° and 40° latitude for the LW and SW AIRS CO_2, and for MBL, where we have the largest disagreement between AIRS and MBL. This plot clearly indicates that the AIRS CO_2 diverges from MBL in late 2004, with agreement appearing to return at the end of 2005. We now concentrate on the time period between the two vertical bar in this figure. It appears that in late 2004, the MBL growth rate almost stopped for several months, while at the same time the AIRS growth rate increased above normal levels. This produced an offset between MBL and AIRS during most of 2005 of almost 2 ppm.

[86] The reasonably good agreement between the SW and LW CO_2 growth rate shown in Figure 21 (before the February 2006 ECMWF change) suggests that the difference between AIRS and MBL is not due to our use of ECMWF for the atmospheric temperature. (This figure does show the relatively large disagreement between the SW and LW AIRS CO_2 starting in February 2006.) A linear least-squares fit to these curves for the growth rates between 1 January 2003 and the left-hand side vertical bar, and a separate fit from the right-hand side vertical bar to 31 December 2005 are shown in Table 1 under AIRS/MBL 20–40° latitude subset. The second column shows the fitted rates for each time series before and after the vertical bars, along with their mean values. We observe that both of the AIRS rates shown are *lower* than the MBL rates, with an average AIRS CO_2 growth rate of 2.21 ppm/year compared to the MBL rate of 2.48 ppm/year. Thus we conclude that the higher rates for AIRS than MBL shown in Figure 20 are mostly due to very different behavior in these two time series during the late fall of 2004. This result increases our confidence in the radiometric stability of AIRS.

[87] The differences between the MBL and AIRS CO_2 growth rates are very small, and diagnosing these observed

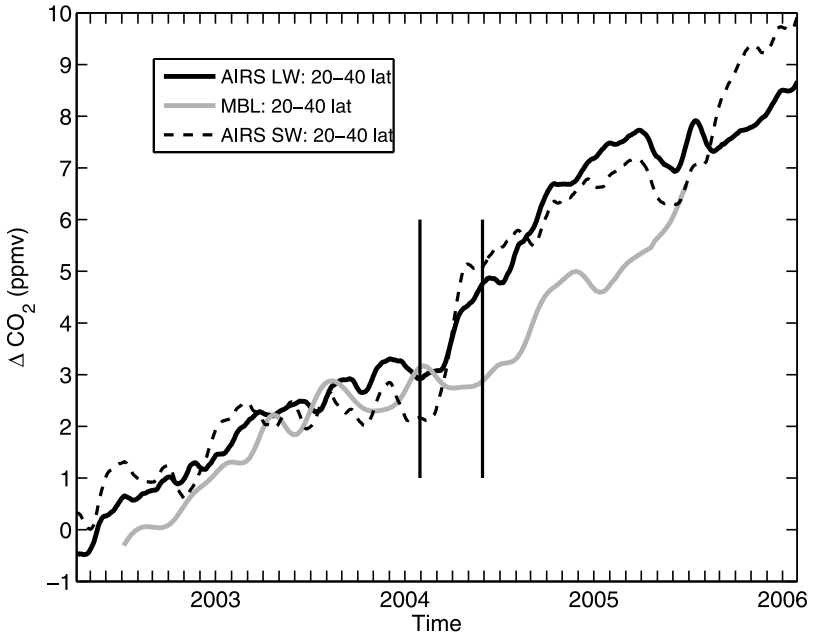

Figure 21. The AIRS LW and SW CO_2 record and the NOAA-ESRL MBL record using deseasonalized data, averaged over 20° to 40° latitude. The two vertical bars indicate a time span when the growth of CO_2 in the oceanic boundary layer (MBL) was significantly different than that in the AIRS-measured CO_2 growth rates for both LW and SW. Table 1 gives the growth rates for AIRS and MBL for times previous to the first vertical bar, times after the second vertical bar, and their average.

small differences is beyond the scope of this paper. It must be kept in mind that these are zonally averaged rates, and both the AIRS and MBL rates are highly likely to weight points differently in the longitude mean. For example, Figure 1 shows that the longitude of clear FOVs varies greatly with latitude. The mean longitude of our observations (using $-180°$ to $+180°$) varies within $\sim\pm30°$ latitude for all latitudes except for the two zones within $\pm2°$ latitude of the equator, which have a mean longitude of $\sim-50°$. Our zonal ocean CO_2 may also have a significant continental influence in the Indian/Arabian sea, where we found a large number of clear FOVs.

[88] A possible source of error for the AIRS CO_2 rates is drift in the AIRS radiometric calibration. *Aumann et al.* [2006] have attempted to address this in the context of validation of the AIRS radiometric accuracy, where he estimated that AIRS is stable to at least 0.016 K/year with a 95% confidence limit, now estimated to be 0.010 K/year by H.H. Aumann (unpublished data, 2007). He used the NOAA RTG-SST sea surface product [*Thiébaux et al.*, 2003] in the tropics as a known temperature to compare to AIRS retrieved SST, using essentially the same clear-FOV subset that we used in this work. His AIRS SST uses the 2616 cm^{-1} channel, which is the most transparent AIRS channel and has essentially no absorption because of CO_2.

[89] We repeated his analysis using our data subset, and the ECMWF SST product, which is stated by ECMWF to be the NCEP SST analysis. Comparisons for one day in 2003 confirm that the NCEP and ECMWF SST are essentially identical. Our subset gives a drift relative to the ECMWF tropical SST of 12 mK ± 15 mK (taking into account autocorrelation of time series), essentially the same result. However, as noted by *Aumann et al.* [2006], the RTA SST record contains an offset in May 2004. We find that our Obs-Calcs with respect to ECMWF SST is +4 mK/year for Sept. 2002 through April 2004, and -6 mK/year for June 2004 through August 2006, both of which are smaller than the drift from the combined 4-year data set which includes the May 2004 RTG SST offset.

[90] This analysis suggests that the AIRS radiometry is stable to at least 10 mK/year, implying a maximum uncertainty of 0.3 ppm/year in the AIRS CO_2 growth rate. At this time, we believe that it is not possible to associate differences in the AIRS and MBL growth rates to any known drift in the AIRS radiometry. In addition, it is highly unlikely that a radiometric drift could cause the latitudinal variability of the CO_2 growth rates shown in Figure 20.

6. Summary and Conclusions

[91] A 4-year zonal CO_2 climatology derived from AIRS for ocean-only measurements was shown to be accurate to $\sim0.5-1$ ppm, at least in the $-20°$ to $+30°$ latitude region where validation data exists. Comparisons to the NOAA GLOBALVIEW MBL CO_2 smoothed product clearly shows the operation of rectifier effect, which limits venting of CO_2 out of the boundary layer in northern latitudes. Comparisons of the phase between the MBL and AIRS CO_2 seasonal cycles may offer some insights into the transport of CO_2 from the northern to southern latitudes. In particular we find that in the deep tropics the AIRS CO_2 leads the MBL CO_2 by $\sim1\frac{1}{2}$ months, presumably because of transport from higher latitudes where the CO_2 seasonal cycle leads the tropical MBL phase.

[92] The observed CO_2 growth rates during the three years 2003–2005, averaged over all latitudes, agree with the MBL growth rates to within 0.38 ppm/year. However, our CO_2 rates are systematically higher than the MBL rates in the mid-latitudes by 0.3–0.5 ppm/year. This appears to be due to some event, or unknown error source, that was in force during late 2004 when the MBL and AIRS CO_2 rates diverged for a short time period.

[93] This work establishes the ability of AIRS to measure global CO_2 concentrations in the mid- to lower-troposphere with high accuracy. By using only very clear FOVs over ocean, our CO_2 climatology is largely unaffected by clouds, which allowed us to use such low-peaking CO_2 channels. Unfortunately, there are limited lower to middle tropospheric validation measurements over ocean; we used two sets of 3.5-km aircraft measurements to partially validate our CO_2 results, with additional partial validation from the more extensive 250 mbar measurement aboard the Pacific JAL airline flights.

[94] There are also questions of how sampling may bias our results. The use of clear only FOVs generally means we have avoided regions of strong convection that might prove interesting for transport studies. In addition, some of our zonal averages come from regions without strong nearby continental flow, while others region might be strongly influenced by continental outflow.

[95] Future studies will include detailed model comparisons, retrievals over land, and possibly the use of AIRS cloud-cleared radiances for the CO_2 measurement. This last possibility could potentially allow more detailed validation by greatly increasing the density of usable data, and hopefully provide enough data to generate meaningful maps, which will help alleviate a sampling bias and possibly provide better transport information as well as information on source and sink regions. Increased data density should also allow us to generate zonal averages from longitudinally gridded data, which would be more statistically representative. In addition, given the potential accuracy of the results presented here, more detailed studies of the effects of residual cloudiness on our derived CO_2 are warranted. This work does, however, appear to represent a vast amount of new global CO_2 data for the mid- to lower-troposphere that will hopefully prove useful to the carbon modeling community.

[96] **Acknowledgments.** This work was funded by NASA Headquarters under grant NNG04GG03G. We would also like acknowledge the efforts of those who made the AIRS instrument possible, especially Moustafa Chahine, Ramesh Kakar, Fred O'Callahan, George Aumann, Tom Pagano, and the BAE team that designed and built AIRS. We also thank Howard Motteler and Sergio De-Souza Machado at UMBC for their contributions to this work.

References

Auligne, T., A. McNally, and D. Dee (2007), Adaptive bias correction for satellite data in a numerical weather prediction system, *Q. J. R. Meteorol. Soc.*, *133*, 631–642, doi:10.1002/qj.56.

Aumann, H., et al. (2003), AIRS/AMSU/HSB on the Aqua mission: Design, science objectives, data products and processing systems, *IEEE Trans. Geosci. Remote Sens.*, *41*, 253–264.

Aumann, H. H., D. Gregorich, and S. Gaiser (2005), AIRS hyper-spectral measurements for climate research: Carbon dioxide and nitrous oxide effects, *Geophys. Res. Lett.*, *32*, L05806, doi:10.1029/2004GL021784.

Aumann, H. H., S. Broberg, D. Elliott, S. Gaiser, and D. Gregorich (2006), Three years of Atmospheric Infrared Sounder radiometric calibration

validation using sea surface temperatures, *J. Geophys. Res.*, *111*, D16S90, doi:10.1029/2005JD006822.

Barkley, M. P., U. Frieß, and P. S. Monks (2006a), Measuring atmospheric CO_2 from space using Full Spectral Initiation (FSI) WFM-DOAS, *Atmos. Chem. Phys.*, *6*, 3517–3534.

Barkley, M. P., P. S. Monks, and R. J. Engelen (2006b), Comparison of SCIAMACHY and AIRS CO_2 measurements over North America during the summer and autumn of 2003, *Geophys. Res. Lett.*, *33*, L20805, doi:10.1029/2006GL026807.

Barkley, M. P., et al. (2007), Assessing the near surface sensitivity of SCIAMACHY atmospheric CO_2 retrieved using (FSI) WFM-DOAS, *Atmos. Chem. Phys.*, *7*, 3597–3619.

Buchwitz, M., O. Schneising, J. P. Burrows, H. Bovensmann, M. Reuter, and J. Notholt (2007a), First direct observation of the atmospheric CO_2 year-to-year increase from space, *Atmos. Chem. Phys.*, *7*, 4249–4256.

Buchwitz, M., O. Schneising, J. P. Burrows, H. Bovensmann, M. Reuter, and J. Notholt (2007b), Corrigendum to "First direct observation of the atmospheric CO_2 year-to-year increase from space", *Atmos. Chem. Phys.*, *7*(20), 5341–5342.

Chahine, M., C. Barnet, E. T. Olsen, L. Chen, and E. Maddy (2005), On the determination of atmospheric minor gases by the method of vanishing partial derivatives with application to CO_2, *Geophys. Res. Lett.*, *32*, L22803, doi:10.1029/2005GL024165.

Chahine, M. T., et al. (2006), AIRS: Improving weather forecasting and providing new data on greenhouse gases, *Bull. Am. Meteorol. Soc.*, *87*, 911–926.

Chédin, A., A. Hollingsworth, N. A. Scott, S. Serrar, C. Crevoisier, and R. Armante (2002), Annual and seasonal variations of atmospheric CO_2, N_2O and CO concentrations retrieved from NOAA/TOVS satellite observations, *Geophys. Res. Lett.*, *29*(8), 1269, doi:10.1029/2001GL014082.

Chédin, A., R. Saunders, A. Hollingsworth, N. Scott, M. Matricardi, J. Etcheto, C. Clerbaux, R. Armante, and C. Crevoisier (2003a), The feasibility of monitoring CO_2 from high-resolution infrared sounders, *J. Geophys. Res.*, *108*(D2), 4064, doi:10.1029/2001JD001443.

Chédin, A., S. Serrar, N. A. Scott, C. Crevoisier, and R. Armante (2003b), First global measurement of midtropospheric CO_2 from NOAA polar satellites: Tropical zone, *J. Geophys. Res.*, *108*(D18), 4581, doi:10.1029/2003JD003439.

Chevallier, F., R. J. Engelen, and P. Peylin (2005), The contribution of AIRS data to the estimation of CO_2 sources and sinks, *Geophys. Res. Lett.*, *32*, L23801, doi:10.1029/2005GL024229.

Crevoisier, C., A. Chedin, and N. Scott (2003), AIRS channel selection for CO_2 and other trace-gas retrievals, *Q. J. R. Meteorol. Soc.*, *129*(593), 2719–2740, doi:10.1256/qj.02.180.

Crevoisier, C., S. Heilliette, A. Chédin, S. Serrar, R. Armante, and N. A. Scott (2004), Midtropospheric CO_2 concentration retrieval from AIRS observations in the tropics, *Geophys. Res. Lett.*, *31*, L17106, doi:10.1029/2004GL020141.

Denning, A. S., I. Y. Fung, and D. Randall (1995), Latitudinal gradient of atmospheric CO_2 due to seasonal exchange with land biota, *Nature*, *376*, 240–243, doi:10.1038/376240a0.

Denning, A. S., G. J. Collatz, C. Zhang, D. A. Randall, J. A. Berry, P. J. Sellers, and D. A. Dazlich (1996), Simulations of terrestrial carbon metabolism and atmospheric CO_2 in a general circulation model: Part 1: Surface carbon fluxes, *Tellus, Ser. B*, *48*, 521–542, doi:10.1034/j.1600-0889.1996.t01-2-00009.x.

Engelen, R. J., and A. P. McNally (2005), Estimating atmospheric CO_2 from advanced infrared satellite radiances within an operational four-dimensional variational (4D-Var) data assimilation system: Results and validation, *J. Geophys. Res.*, *110*, D18305, doi:10.1029/2005JD005982.

Engelen, R. J., E. Andersson, F. Chevallier, A. Hollingsworth, M. Matricardi, A. P. McNally, J.-N. Thépaut, and P. D. Watts (2004), Estimating atmospheric CO_2 from advanced infrared satellite radiances within an operational 4D-Var data assimilation system: Methodology and first results, *J. Geophys. Res.*, *109*, D19309, doi:10.1029/2004JD004777.

Ghil, M., et al. (2002), Advanced spectral methods for climatic time series, *Rev. Geophys.*, *40*(1), 1003, doi:10.1029/2000RG000092.

GLOBALVIEW-CO2 (2006), Cooperative Atmospheric Data Integration Project—Carbon Dioxide [CD-ROM], *Tech. rep.*, NOAA ESRL, Boulder, Colo. (Also available on Internet via anonymous FTP to ftp.cmdl.noaa.gov, Path: ccg/co2/GLOBALVIEW)

Gurney, K. R., et al. (2003), TransCom 3 CO_2 inversion intercomparison. 1: Annual mean control results and sensitivity to transport and prior flux information, *Tellus, Ser. B*, *55*, 555–579, doi:10.1034/j.1600-0889.2003.00049.x.

Houweling, S., W. Hartmann, I. Aben, H. Schrijver, J. Skidmore, G.-J. Roelofs, and F.-M. Breon (2005), Evidence of systematic errors in SCIAMACHY-observed CO_2 due to aerosols, *Atmos. Chem. Phys.*, *5*, 3003–3013.

Kondrashov, D., and M. Ghil (2006), Spatio-temporal filling of missing points in geophysical data sets, *Nonlinear Proc. Geophys.*, *13*, 151–159.

Masuda, K., T. Takashima, and Y. Takayama (1988), Emissivity of pure and sea waters for the model sea surface in the infrared window regions, *Remote Sens. Environ.*, *24*, 313–329.

Matsueda, H., H. Yoshikawa Inoue, and M. Ishii (2002), Aircraft observation of carbon dioxide at 8–13 km altitude over the western Pacific from 1993 to 1999, *Tellus, Ser. B*, *54*, 1–21, doi:10.1034/j.1600-0889.2002.00304.x.

Nakazawa, T., K. Miyashita, S. Aoki, and M. Tanaka (1991), Temporal and spatial variations of upper tropospheric and lower stratospheric carbon dioxide, *Tellus, Ser. B*, *43*, 106–117.

Pagano, T., H. Aumann, D. Hagan, and K. Overoye (2003), Prelaunch and in-flight radiometric calibration of the atmospheric infrared sounder (AIRS), *IEEE Trans. Geosci. Remote Sens.*, *41*(2), 265–273, doi:10.1109/TGRS.2002.808324.

Peters, W., et al. (2007), An atmospheric perspective on North American carbon dioxide exchange: CarbonTracker, *Proc. Natl. Acad. Sci. U.S.A.*, *104*(48), 18,925–18,930, doi:10.1073/pnas.0708986104.

Raupach, M. R., G. Marland, P. Ciais, C. Le Quere, J. G. Canadell, G. Klepper, and C. B. Field (2007), Global and regional drivers of accelerating CO_2 emissions, *Proc. Natl. Acad. Sci. U.S.A.*, *104*(24), 10,288–10,293, doi:10.1073/pnas.0700609104.

Rothman, L. S., et al. (2005), The HITRAN 2004 molecular spectroscopic database, *J. Quant. Spectrosc. Radiat. Transfer*, *96*, 139–204, doi:10.1016/j.jqsrt.2004.10.008.

Santer, B. D., T. M. L. Wigley, J. S. Boyle, D. J. Gaffen, J. J. Hnilo, D. Nychka, D. E. Parker, and K. E. Taylor (2000), Statistical significance of trends and trend differences in layer-average atmospheric temperature time series, *J. Geophys. Res.*, *105*, 7337–7356.

Stephens, B. B., et al. (2007), Weak northern and strong tropical land carbon uptake from vertical profiles of atmospheric CO_2, *Science*, *316*, 1732–1735, doi:10.1126/science.1137004.

Strahan, S. E., A. R. Douglass, J. E. Nielsen, and K. A. Boering (1998), The CO_2 seasonal cycle as a tracer of transport, *J. Geophys. Res.*, *103*, 13,729–13,742.

Strow, L. L., S. E. Hannon, S. de Souza-Machado, H. E. Motteler, and D. Tobin (2003), An overview of the AIRS radiative transfer model, *IEEE Trans. Geosci. Remote Sens.*, *41*, 303–313, doi:10.1109/TGRS.2002.808244.

Strow, L. L., S. E. Hannon, S. De-Souza Machado, H. E. Motteler, and D. C. Tobin (2006), Validation of the Atmospheric Infrared Sounder radiative transfer algorithm, *J. Geophys. Res.*, *111*, D09S06, doi:10.1029/2005JD006146.

Thiébaux, J., E. Rogers, W. Wang, and B. Katz (2003), A new high-resolution blended real-time global sea surface temperature analysis, *Bull. Am. Meteorol. Soc.*, *84*, 645–656.

Tiwari, Y. K., M. Gloor, R. J. Engelen, F. Chevallier, C. Rödenbeck, S. Körner, P. Peylin, B. H. Braswell, and M. Heimann (2006), Comparing CO_2 retrieved from Atmospheric Infrared Sounder with model predictions: Implications for constraining surface fluxes and lower-to-upper troposphere transport, *J. Geophys. Res.*, *111*, D17106, doi:10.1029/2005JD006681.

Yang, Z., R. A. Washenfelder, G. Keppel-Aleks, N. Y. Krakauer, J. T. Randerson, P. P. Tans, C. Sweeney, and P. O. Wennberg (2007), New constraints on Northern Hemisphere growing season net flux, *Geophys. Res. Lett.*, *34*, L12807, doi:10.1029/2007GL029742.

S. E. Hannon and L. L. Strow, Physics Department and Joint Center for Earth Systems Technology, University of Maryland Baltimore County, 1000 Hilltop Circle, Baltimore, MD 21250, USA. (strow@umbe.edu)